AD-A067 787 ILLINOIS UNIV AT URBANA-CHAMPAIGN ELECTROMAGNETICS LAB F/G 9/5
SOURCE EXCITATION OF AN OPEN, PARALLEL-PLATE WAVEGUIDE. NUMERIC--ETC(U)
AUG 78 V KRICHEVSKY AFOSR-76-3066
UNCLASSIFIED UIEM-78-4 AFOSR-TR-79-0431 NL

| OF |
AD
A067 787

END
DATE FILMED
6 -79
DDC

ELECTROMAGNETICS LABORATORY
SCIENTIFIC REPORT NO. 78-4

August 1978

12

LEVEL II

SOURCE EXCITATION OF AN OPEN, PARALLEL-PLATE WAVEGUIDE. NUMERICAL RESULTS

V. Krichevsky

ELECTROMAGNETICS LABORATORY
DEPARTMENT OF ELECTRICAL ENGINEERING
ENGINEERING EXPERIMENT STATION
UNIVERSITY OF ILLINOIS AT URBANA-CHAMPAIGN
URBANA, ILLINOIS 61801

Supported by
Grant No. 76-3066B
Air Force Office
of Scientific Research
Bolling AFB
Washington, D.C. 20332

AIR FORCE OFFICE OF SCIENTIFIC RESEARCH (AFSC)
NOTICE OF TRANSMITTAL TO DDC
This t[illegible] reviewed and is
approved for public release IAW AFR 190-12 (7b).
Distribution is unlimited.
A. D. Blose
Technical Information Officer

UNCLASSIFIED

SECURITY CLASSIFICATION OF THIS PAGE (When Data Entered)

REPORT DOCUMENTATION PAGE	READ INSTRUCTIONS BEFORE COMPLETING FORM
1. REPORT NUMBER: AFOSR-TR-79-0431	2. GOVT ACCESSION NO. / 3. RECIPIENT'S CATALOG NUMBER
4. TITLE (and Subtitle): SOURCE EXCITATION OF AN OPEN, PARALLEL-PLATE WAVEGUIDE. NUMERICAL RESULTS.	5. TYPE OF REPORT & PERIOD COVERED: Interim rept.
	6. PERFORMING ORG. REPORT NUMBER: EM-78-4, UILU-ENG-78-2546
7. AUTHOR(s): V. Krichevsky	8. CONTRACT OR GRANT NUMBER(s): AFOSR-76-3066
9. PERFORMING ORGANIZATION NAME AND ADDRESS: Electromagnetics Laboratory, Department of Electrical Engineering, University of Illinois, Urbana, Illinois 61801	10. PROGRAM ELEMENT, PROJECT, TASK AREA & WORK UNIT NUMBERS: 2301 A3, 61102F
11. CONTROLLING OFFICE NAME AND ADDRESS: Air Force Office of Scientific Research/NP, Building 410, Bolling AFB, Washington, DC 20332	12. REPORT DATE: Aug[illegible]78
	13. NUMBER OF PAGES: 56
14. MONITORING AGENCY NAME & ADDRESS(if different from Controlling Office)	15. SECURITY CLASS. (of this report): Unclassified
	15a. DECLASSIFICATION/DOWNGRADING SCHEDULE

16. DISTRIBUTION STATEMENT (of this Report)

Approved for public release;
distribution unlimited.

17. DISTRIBUTION STATEMENT (of the abstract entered in Block 20, if different from Report)

18. SUPPLEMENTARY NOTES

19. KEY WORDS (Continue on reverse side if necessary and identify by block number)

EM Field
Open Parallel-Plate Waveguide
Source Excitation Problem
Numerical Results

20. ABSTRACT (Continue on reverse side if necessary and identify by block number)

In this work we investigate numerically the problem of the source excitation of an open, parallel-plate waveguide. The following assumptions are made for the source current 1) the current is oriented in the y-direction, 2) it is located at $x = 0$, 3) there is no variation in the y-direction, 4) and the current has $\exp(i\beta z)$ behavior along the

408 102 (over)

longitudinal z-direction. We provide graphical output for the EM-field components as functions of a longitudinal propagation constant and transverse coordinates and then discuss these results.

UILU-ENG-78-2546

Electromagnetics Laboratory Report No. 78-4

SOURCE EXCITATION OF AN OPEN, PARALLEL-PLATE WAVEGUIDE. NUMERICAL RESULTS

by

V. Krichevsky

Scientific Report

August 1978

Supported by

Grant No. 76-3066B
Air Force Office of Scientific Research
Bolling AFB, Washington, D.C. 20332

Electromagnetics Laboratory
Department of Electrical Engineering
Engineering Experiment Station
University of Illinois at Urbana-Champaign
Urbana, Illinois 61801

ACKNOWLEDGEMENT

The author is thankful to Professor R. Mittra for discussion of the problem and for the helpful suggestions during the course of this work. The financial support of AFOSR Grant-76-3066B is gratefully acknowledged.

ABSTRACT

In this work we investigate numerically the problem of the source excitation of an open, parallel-plate waveguide. The following assumptions are made for the source current 1) the current is oriented in the y-direction, 2) it is located at x = 0, 3) there is no variation in the y-direction, 4) and the current has exp (iβz) behavior along the longitudinal z-direction. We provide graphical output for the EM-field components as functions of a longitudinal propagation constant and transverse coordinates and then discuss these results.

TABLE OF CONTENTS

LIST OF FIGURES

Figure | Page

I. INTRODUCTION

In the previous report [1], we derived analytical expressions for the source excitation of an open parallel-plate waveguide. However, these formulas were very complicated, and it became necessary to evaluate them numerically. The purpose of this report is to present the numerical results. The computer program contained in Appendix A was written and used to obtain the field distribution as a function of the longitudinal propagation constant and the transverse coordinates. The numerical outputs are presented in graphical forms. The Cyber 175 at the University of Illinois was used for all of the numerical studies.

The organization of the report is as follows: Section II contains a statement of the problem and the basic formulation. Section III presents the real and imaginary parts and the amplitude of the component field distribution as functions of several parameters in graphical form and a detailed discussion of the numerical results. Finally, Section IV is the conclusion.

II. STATEMENT OF THE PROBLEM AND BASIC FORMULATION

In this section the fields due to a vertical current located inside an open, finite waveguide are investigated. The geometry of the problem considered is shown in Figure 1. This structure consists of two perfectly conducting plates with separation 2H located in a homogeneous and isotropic medium. A Cartesian coordinate system with its y-axis normal to the plates is erected. Both plates are infinite in the z-direction and finite in the x-direction with length 2L as shown in Figure 1. All figures appear at the end of Chapter II. The current is oriented in the y-direction and is defined as

$$J = \hat{y}\delta(x) \exp(i\beta z) \quad , \tag{1}$$

where β is the propagation constant in the z-direction, and $\delta(x)$ is the delta function. In [1] using the vector-potential approach and the Wiener-Hopf technique, we obtained a solution for the problem at hand in a general form for any parameters with one restriction: kL must be much greater than 1, i.e.,

$$kL \gg 1 \quad , \tag{2}$$

where

$$k = \sqrt{\omega^2\varepsilon\mu - \beta^2} \tag{3}$$

and ε, μ are the homogeneous media parameters. Using the solution which was obtained in [1], we will perform a numerical calculation for the case:

$$W = \frac{H}{L} = 0.16670 \quad , \tag{4}$$

$$\frac{L}{\lambda_0} = 5 \quad , \tag{5}$$

where

$$\lambda_0 = \frac{2\pi}{\omega\sqrt{\varepsilon\mu}} \tag{6}$$

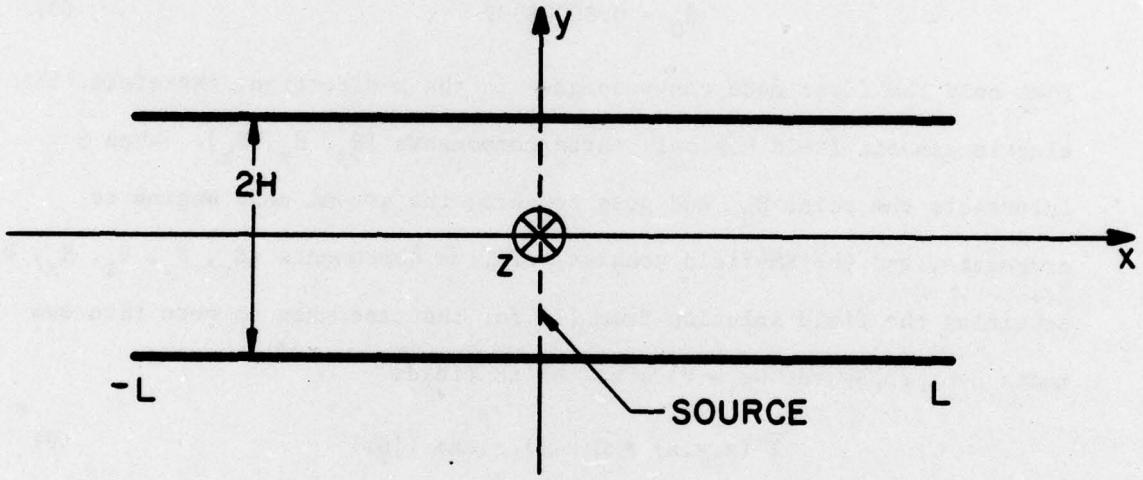

Figure 1. Geometry of the problem of source excitation of a parallel-plate waveguide.

is the free-space wave length. Because of the limitations of Equations (2), (3), and (5) we calculated numerical results for

$$0 < \tilde{\beta} < 0.93 \quad , \tag{7}$$

where $\tilde{\beta}$ is the normalized propagation constant $\tilde{\beta} = \frac{\beta}{\omega\sqrt{\varepsilon\mu}}$. It can be readily proved from Equations (3), (4), and (5) that if $\tilde{\beta}$ is in the region $[\tilde{\beta}_0, 0.93]$, where

$$\tilde{\beta}_0 = 0.80008997 \quad , \tag{8}$$

then only the first mode can propagate in the x-direction; therefore, the electromagnetic field has only three components $[E_y, H_x, H_z]$. When $\tilde{\beta}$ intersects the point $\tilde{\beta}_0$ and goes to zero, the second mode begins to propagate, and the EM-field consists of five components $[E_x, E_y, E_z, H_x, H_z]$. Rewriting the field solution from [1] for the case, when no more than two modes can propagate, we arrive at the EM field:

$$\bar{E}'(x,y,z) = \bar{E}(x,y) \cdot \exp(i\beta z) \tag{9}$$

$$\bar{H}'(x,y,z) = \bar{H}(x,y) \cdot \exp(i\beta z) \tag{10}$$

$$\bar{E}(x,y) = \hat{x}E_x + \hat{y}E_y + \hat{z}E_z \tag{11}$$

$$\bar{H}(x,y) = \hat{x}H_x + \hat{z}H_z \tag{12}$$

$$E_y = \sqrt{\frac{\mu}{\varepsilon}} \cdot \frac{0.1 \cdot \theta}{w} \cdot F_2 \sin\left(\frac{\pi}{H}y\right) \sin\left(\theta \cdot \frac{x}{L}\right) \tag{13}$$

$$E_y = \sqrt{\frac{\mu}{\varepsilon}} \cdot 10\pi \left\{ F_1 \cos\left(a \cdot \frac{x}{L}\right) + \left(1 - \frac{0.01}{w^2}\right) \cdot F_2 \cos\left(\frac{\pi}{H}y\right) \cos\left(\theta \cdot \frac{x}{L}\right) - \frac{1}{2a} \exp\left(ia\left|\frac{x}{L}\right|\right) \right\} \tag{14}$$

$$E_z = -i\sqrt{\frac{\mu}{\varepsilon}} \cdot \frac{\beta}{\omega\sqrt{\varepsilon\mu}} \cdot \frac{\pi}{w} F_2 \sin\left(\pi\frac{y}{H}\right) \cos\left(\theta \cdot \frac{x}{L}\right) \quad , \tag{15}$$

$$H_x = -\mu \frac{\beta}{\omega\sqrt{\varepsilon\mu}} \cdot 10\pi \left\{ F_1 \cos\left(a\frac{x}{L}\right) + F_2 \cos\left(\pi \cdot \frac{y}{H}\right) \cdot \cos\left(\theta \cdot \frac{x}{L}\right) - \frac{1}{2a} \exp\left(ia\left|\frac{x}{L}\right|\right) \right\} , \tag{16}$$

$$H_z = i\mu a F_1 \sin\left(a\frac{x}{L}\right) + i\theta F_2 \cos\left(\pi\frac{y}{H}\right) \sin\left(\theta \cdot \frac{x}{L}\right) - 0.5 \cdot \exp\left(ia\left|\frac{x}{L}\right|\right) \cdot \left|\frac{x}{x}\right| , \tag{17}$$

where

$$F_1 = \frac{[M_{1+}(k)]^2 \exp(i2a)}{(1 + T_1)a} \cdot \left\{ 1 + \frac{2b[M_{1+}(\alpha_1)]^2 \exp\left(i2\frac{a}{b}\alpha_1\right)}{\theta} \right\} , \tag{18}$$

$$F_2 = \frac{2bM_{1+}(k)M_{1+}(\alpha_1) \exp\left[ia\left(1 + \frac{\alpha_1}{b}\right)\right]}{a \cdot Q} , \tag{19}$$

$$Q = (1 + T_1)\alpha_1 \cdot \left\{ \frac{[M_{1+}(\alpha_1)]^2 \exp\left(i2\frac{a}{b}\alpha_1\right)}{2\alpha_1} \left[\frac{4T_1 b}{1 + T_1} - \frac{(\alpha_1 + b)^2}{\alpha_1} \right] - 1 \right\} , \tag{20}$$

$$M_{+1}(k) = (\alpha_1 + b) \cdot \exp\left\{ i\left[b\left(2 - C + \ln\left(\frac{2}{b}\right) + i\frac{\pi}{2}\right) - \frac{\pi}{2} + \sum_{n=2}^{\infty} \left(\frac{b}{n} - \arcsin\frac{b}{n}\right) \right] \right\} , \tag{21}$$

$$M_{1+}(\alpha_1) = \sqrt{2} \cdot \alpha_1 \cdot \frac{1 - i\alpha_1}{b} \exp\left\{ i\left[\alpha_1\left(2 - C + \ln\left(\frac{2}{b}\right) + i\frac{\pi}{2}\right) + \sum_{n=2}^{\infty} \left(\frac{\alpha_1}{n} - \arcsin\frac{\alpha_1}{\sqrt{n^2 - 1}} \right) \right] \right\} , \tag{22}$$

$$\alpha_1 = \sqrt{b^2 - 1} , \tag{23}$$

$$a = kL = 10\pi \sqrt{1 - \left(\frac{\beta}{\omega\sqrt{\varepsilon\mu}}\right)^2} , \tag{24}$$

$$b = a \cdot \frac{W}{\pi} , \tag{25}$$

$$\theta = \frac{\pi\alpha_1}{W} , \tag{26}$$

$$T_1 = [M_{1+}(k)]^2 \exp(i2a)\left[1 + \frac{b\sqrt{\pi}}{\sqrt{a}} \exp(-i\frac{\pi}{4})\right] \quad . \qquad (27)$$

It should be mentioned that we investigated the lossless medium case; therefore, in the region $\tilde{\beta}_0 < \tilde{\beta} < 0.93$, the propagation constant for the second mode has only an imaginary part. Because we neglect terms which decrease exponentially, our results for the above mentioned region of $\tilde{\beta}$ reduce to:

1) $E_x = E_z = 0$ and

2) more simple expressions for the other three components of the field.

We apply numerical analysis only over the regions $0 \leq y < H$, $0 < x < L$. For the remainder of the waveguide, one can obtain results using the correlations:

$$E_x(x,y) = -E_x(-x,y) \; ; \; E_x(x,y) = -E_x(x,-y)$$

$$E_y(x,y) = E_y(-x,y) \; ; \; E_y(x,y) = E_y(x,-y)$$

$$E_z(x,y) = E_z(-x,y) \; ; \; E_z(x,y) = -E_z(x,-y)$$

$$H_x(x,y) = H_x(-x,y) \; ; \; H_x(x,y) = H_x(x,-y)$$

$$H_z(x,y) = -H_z(-x,y) \; ; \; H_z(x,y) = H_z(x,-y) \quad . \qquad (28)$$

It is interesting to note that E_x, H_z are continuous and that E_y, E_z, H_x are discontinuous when $\tilde{\beta}$ crosses $\tilde{\beta}_0$ (or more exactly: they are exponentially decreasing). It is also of interest to determine the character of the behavior of the x-component of Poynting's vector. As one can easily see from the previous expressions for the EM fields, the x-component of Poynting's vector for the second mode is proportional to α_1 and goes to zero when $\tilde{\beta} \to \tilde{\beta}_0$. From this, one finds that the energy flow in the x-direction is continuous when $\tilde{\beta}$ intersects the point $\tilde{\beta}_0$.

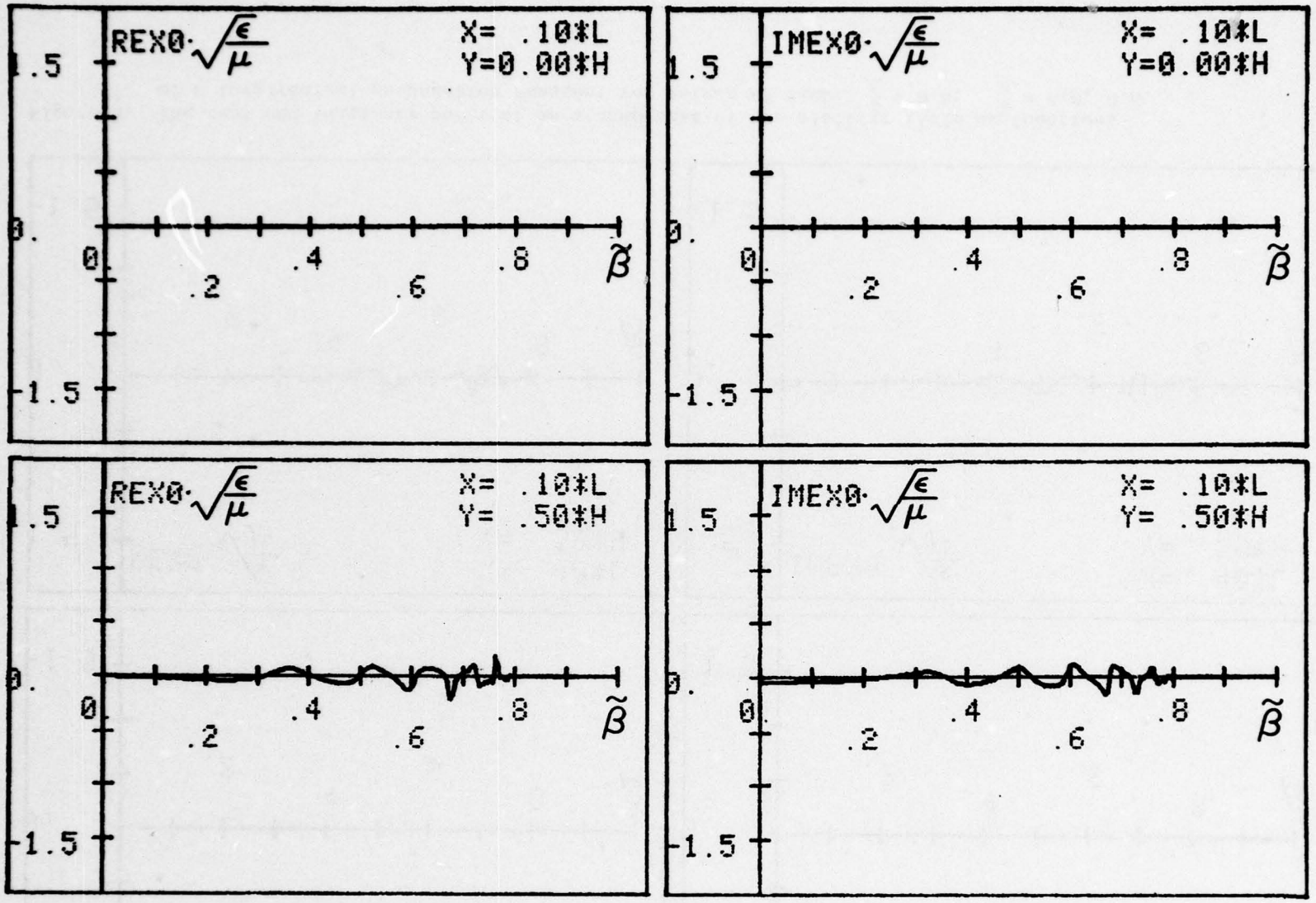

Figure 2. The real and imaginary parts of an x-component of the electric field as functions of a longitudinal propagation constant for points of view: $\frac{x}{L} = 0.1$; $\frac{y}{H} = 0.0, 0.5$.

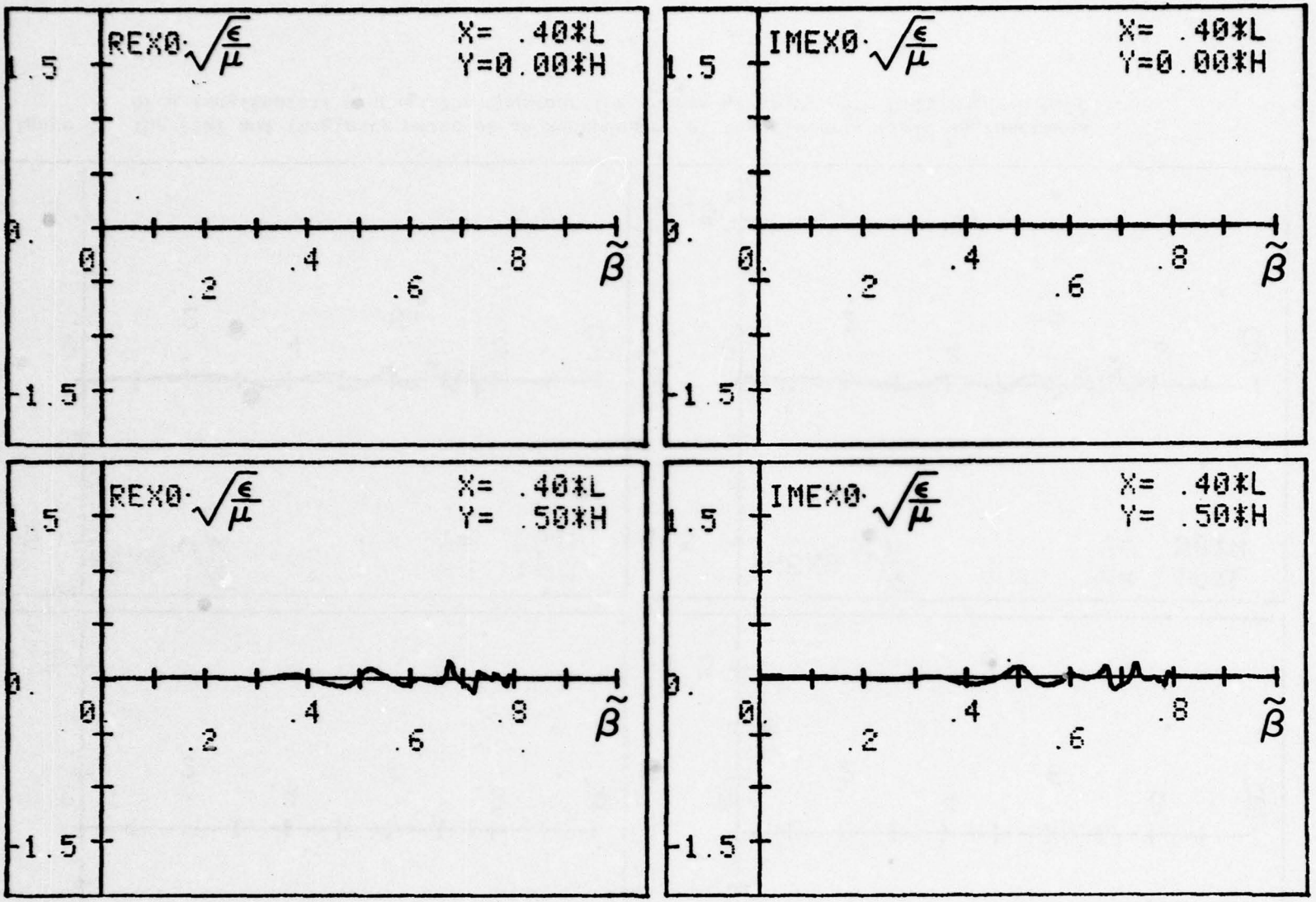

Figure 3. The real and imaginary parts of an x-component of the electric field as functions of a longitudinal propagation constant for points of view: $\frac{X}{L} = 0.4$; $\frac{Y}{H} = 0.0, 0.5$.

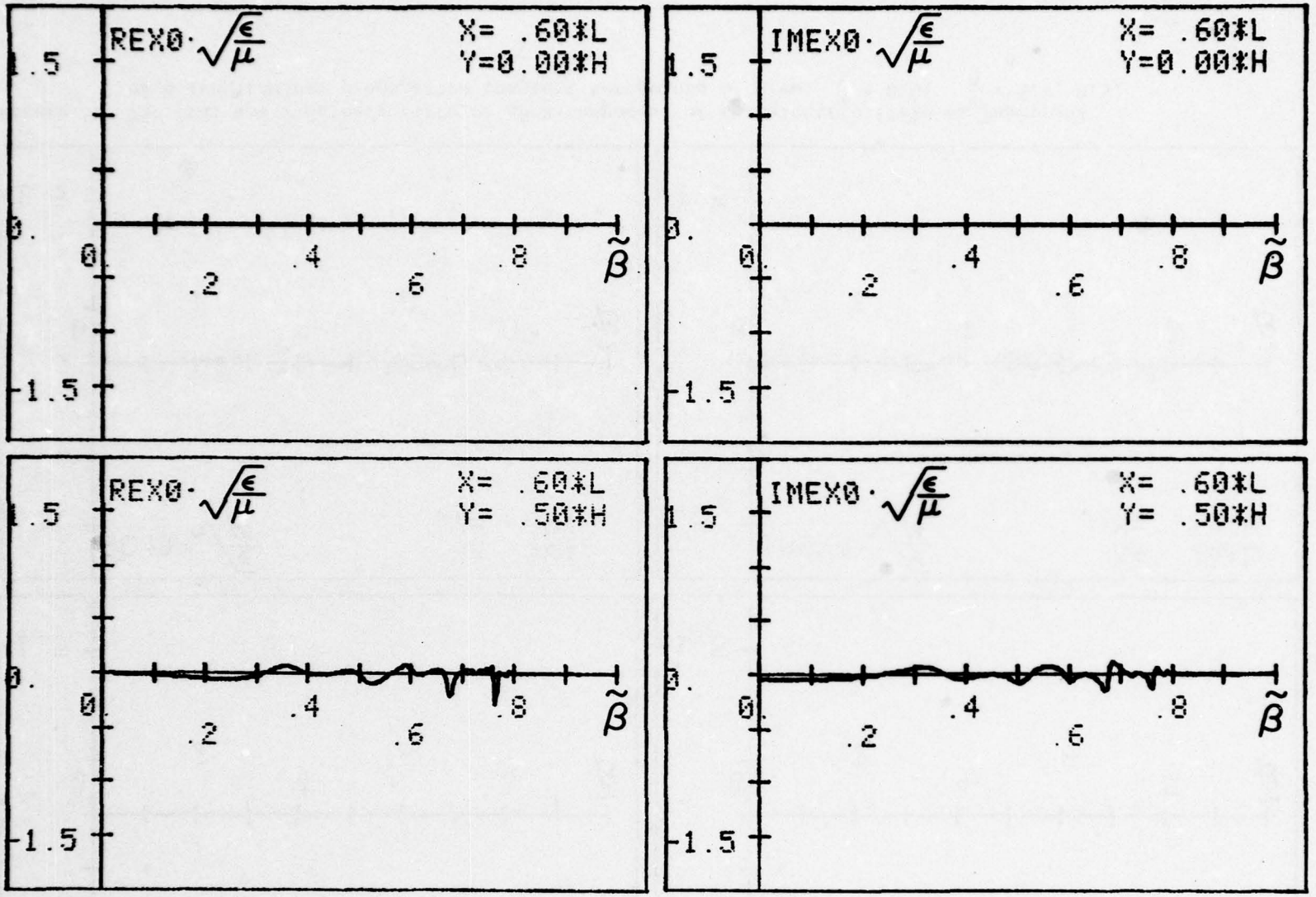

Figure 4. The real and imaginary parts of an x-component of the electric field as functions of a longitudinal propagation constant for points of view: $\frac{x}{L} = 0.6$; $\frac{Y}{H} = 0.0, 0.5$.

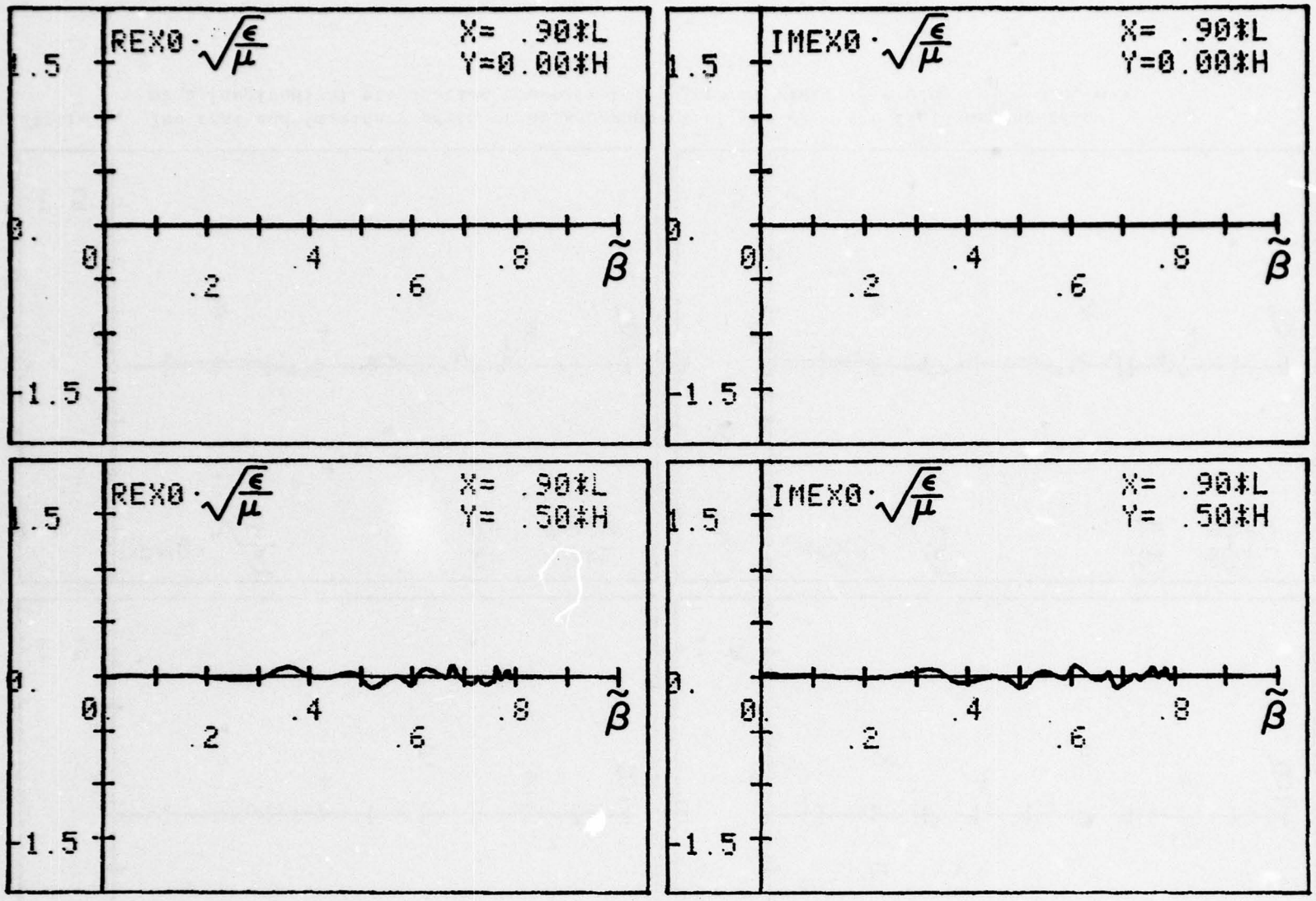

Figure 5. The real and imaginary parts of an x-component of the electric field as functions of a longitudinal propagation constant for points of view: $\frac{x}{L} = 0.9$; $\frac{Y}{H} = 0.0, 0.5$.

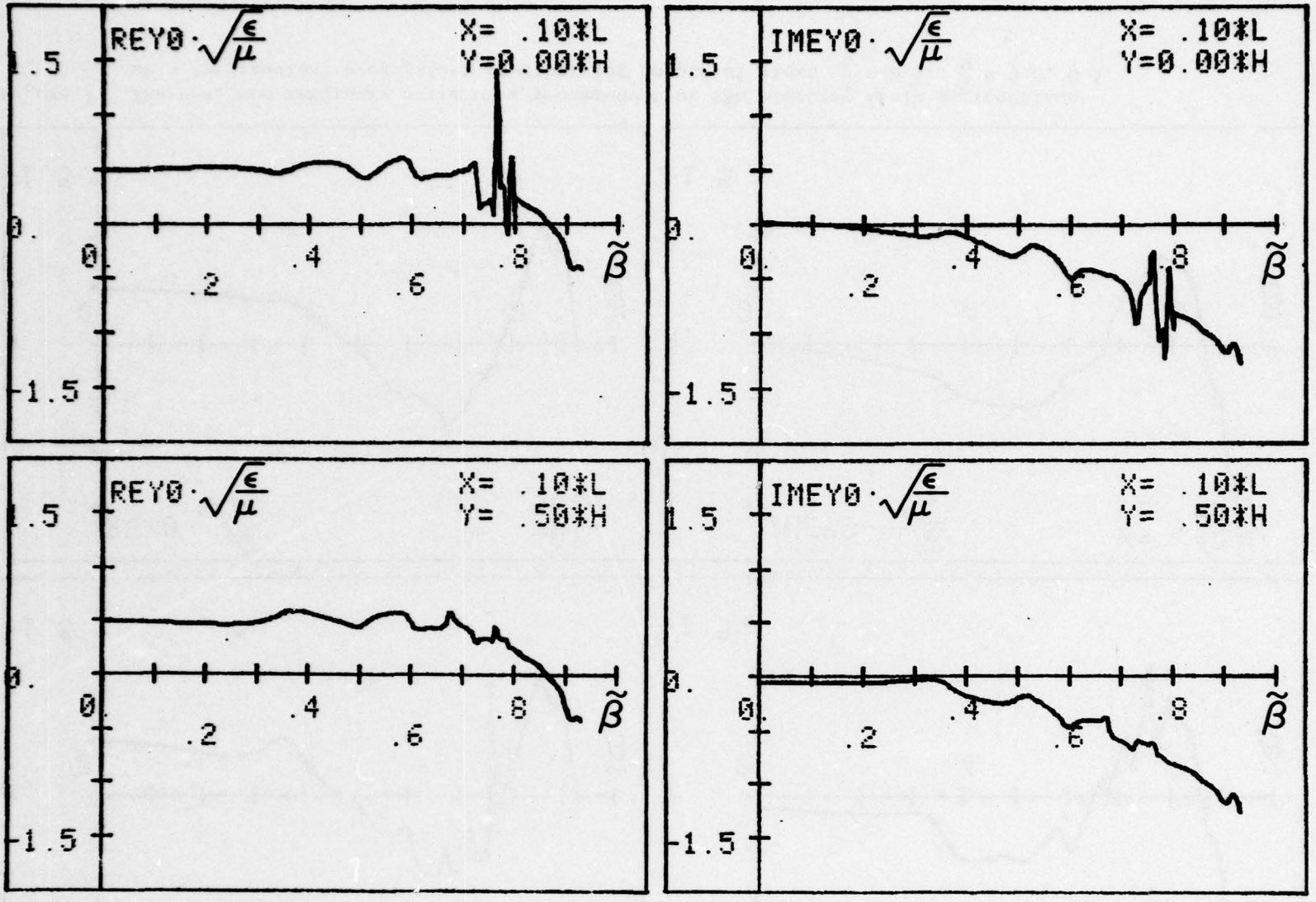

Figure 6. The real and imaginary parts of a y-component of the electric field as functions of a longitudinal propagation constant for points of view: $\frac{x}{L} = 0.1$; $\frac{Y}{H} = 0.0, 0.5$.

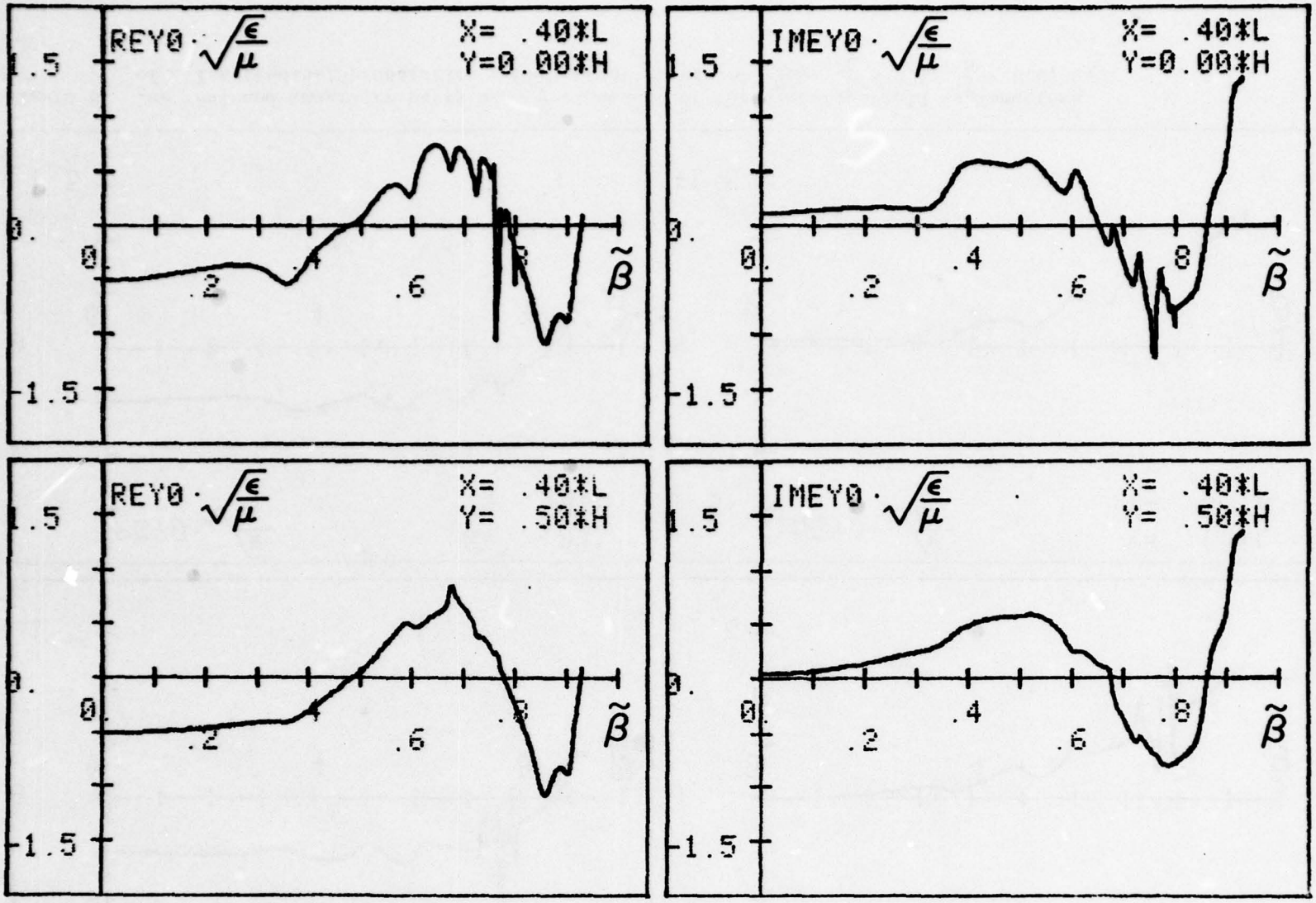

Figure 7. The real and imaginary parts of a y-component of the electric field as functions of a longitudinal propagation constant for points of view: $\frac{x}{L} = 0.4$; $\frac{Y}{H} = 0.0, 0.5$.

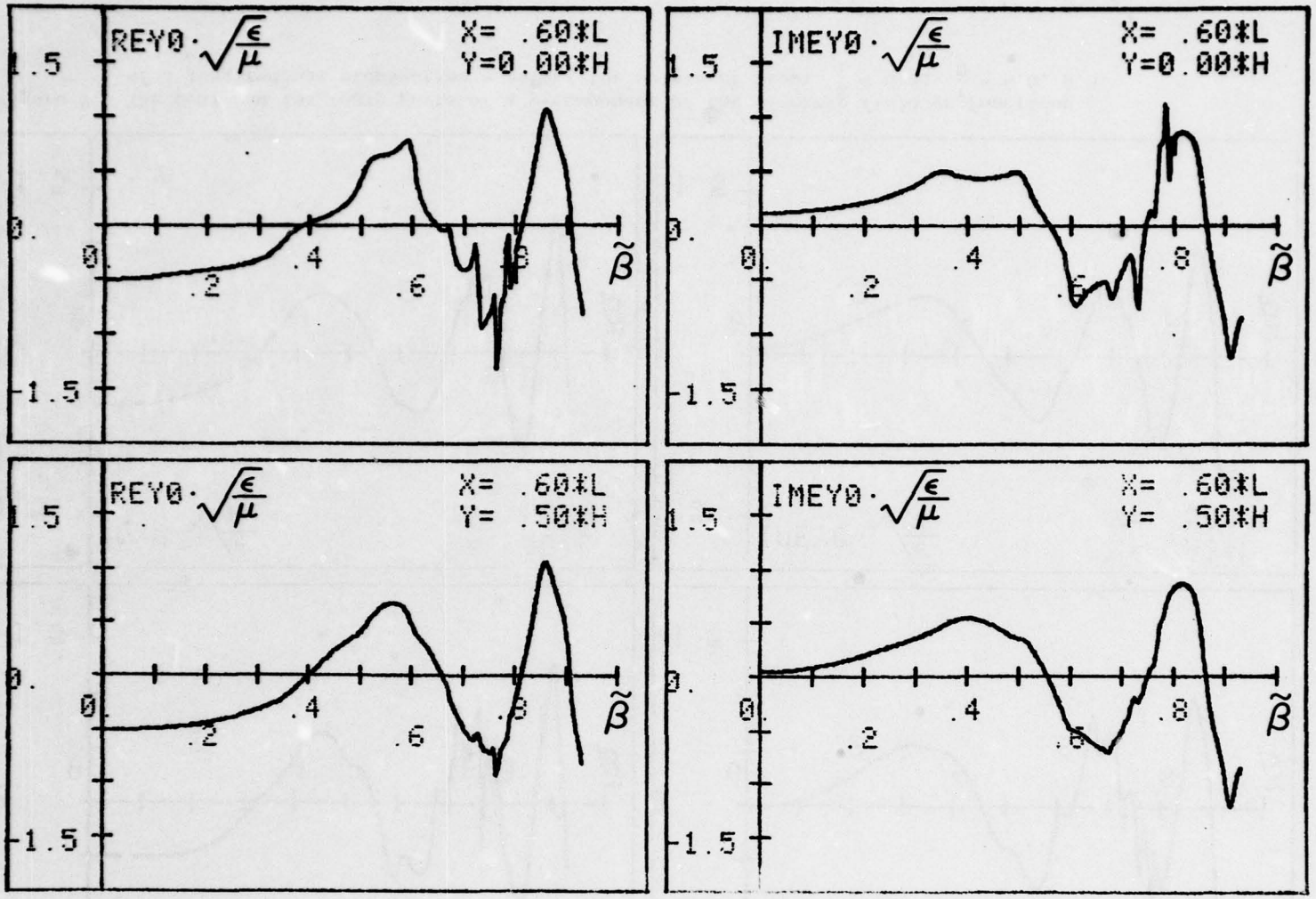

Figure 8. The real and imaginary parts of a y-component of the electric field as functions of a longitudinal propagation constant for points of view: $\frac{x}{L} = 0.6$; $\frac{Y}{H} = 0.0, 0.5$.

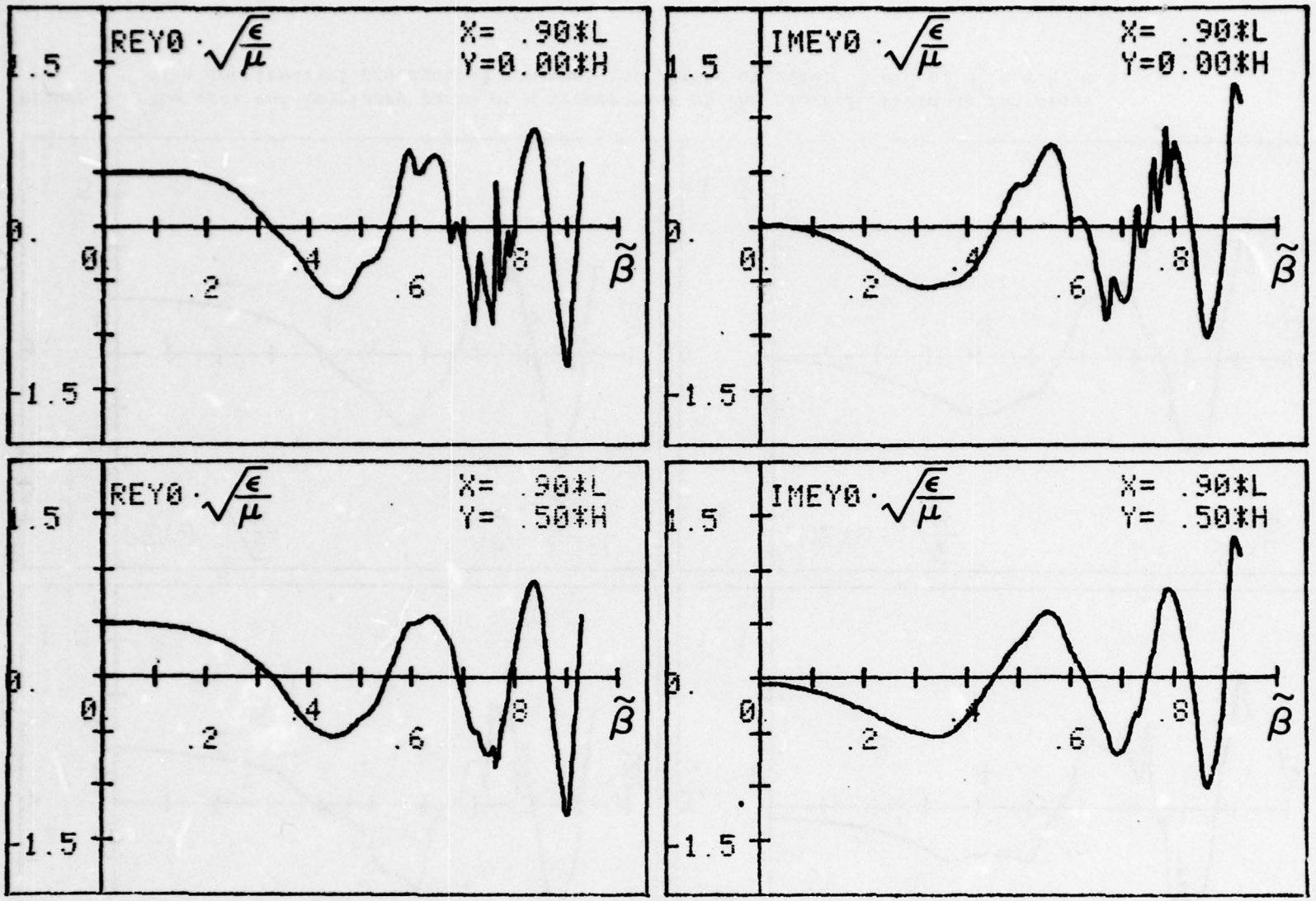

Figure 9. The real and imaginary parts of a y-component of the electric field as functions of a longitudinal propagation constant for points of view: $\frac{x}{L} = 0.9$; $\frac{Y}{H} = 0.0, 0.5$.

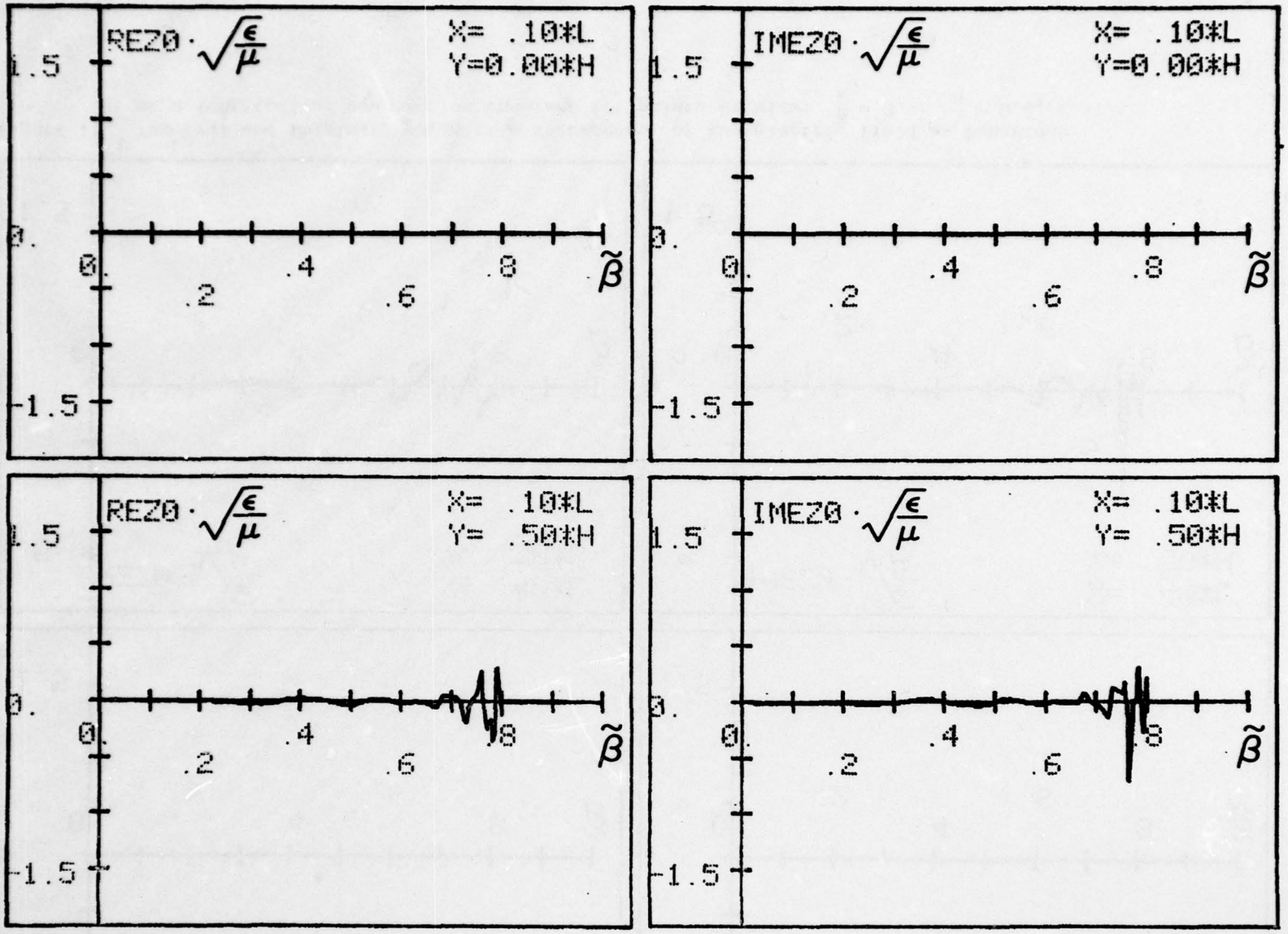

Figure 10. The real and imaginary parts of a z-component of the electric field as functions of a longitudinal propagation constant for points of view: $\frac{x}{L} = 0.1$; $\frac{Y}{H} = 0.0, 0.5$.

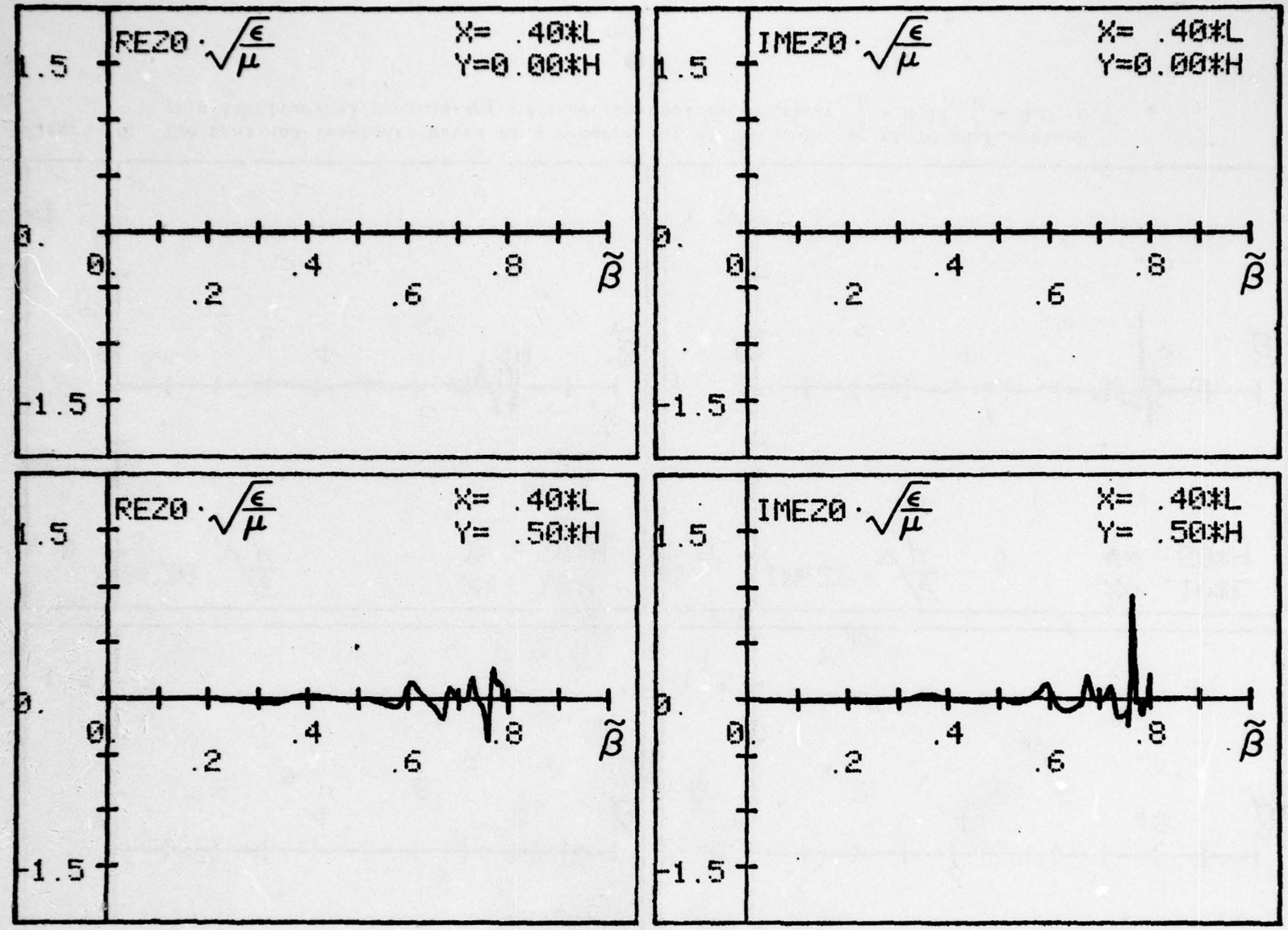

Figure 11. The real and imaginary parts of a z-component of the electric field as functions of a longitudinal propagation constant for points of view: $\frac{x}{L} = 0.4$; $\frac{Y}{H} = 0.0, 0.5$.

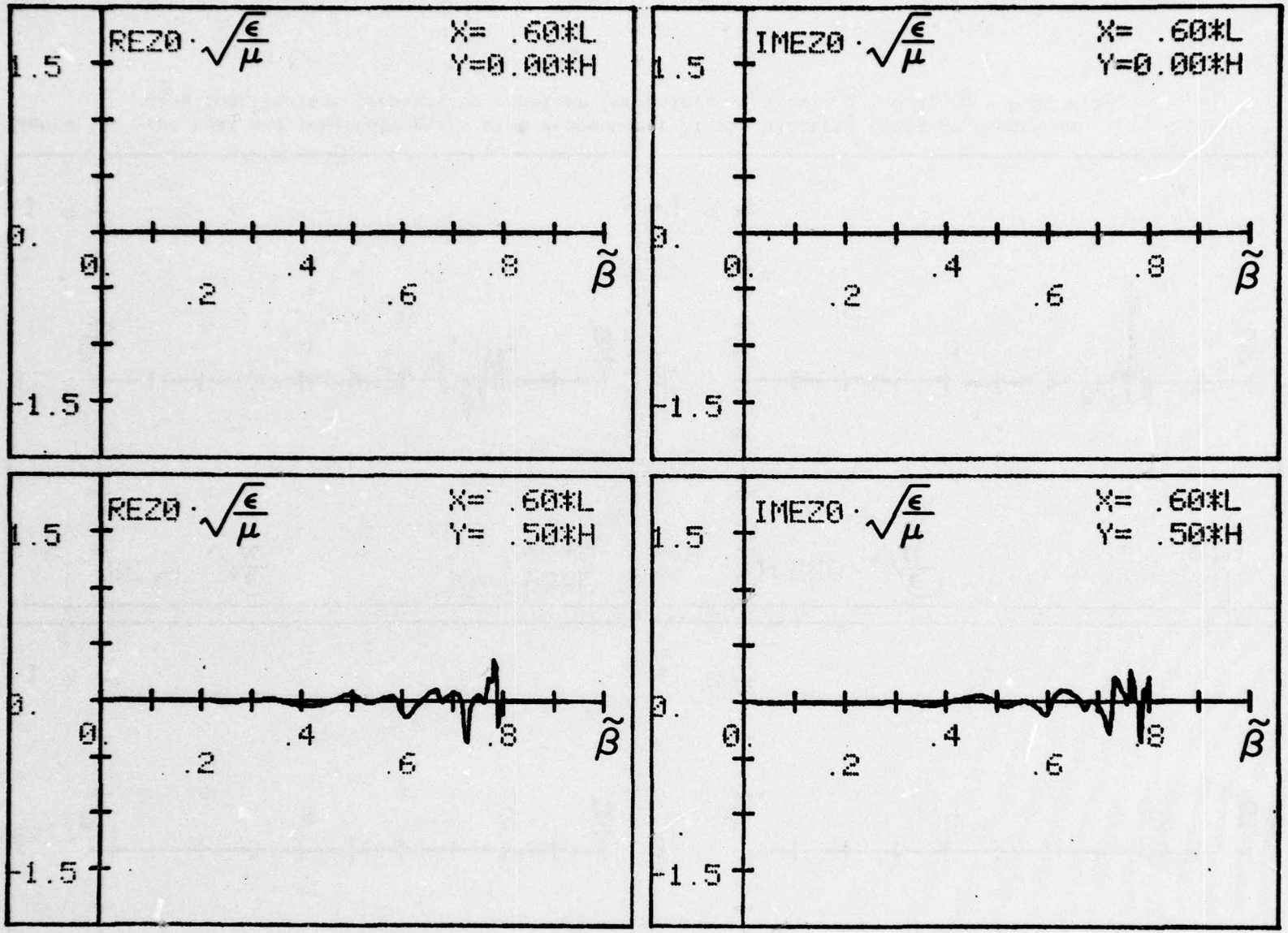

Figure 12. The real and imaginary parts of a z-component of the electric field as functions of a longitudinal propagation constant for points of view: $\frac{x}{L} = 0.6$; $\frac{y}{H} = 0.0, 0.5$.

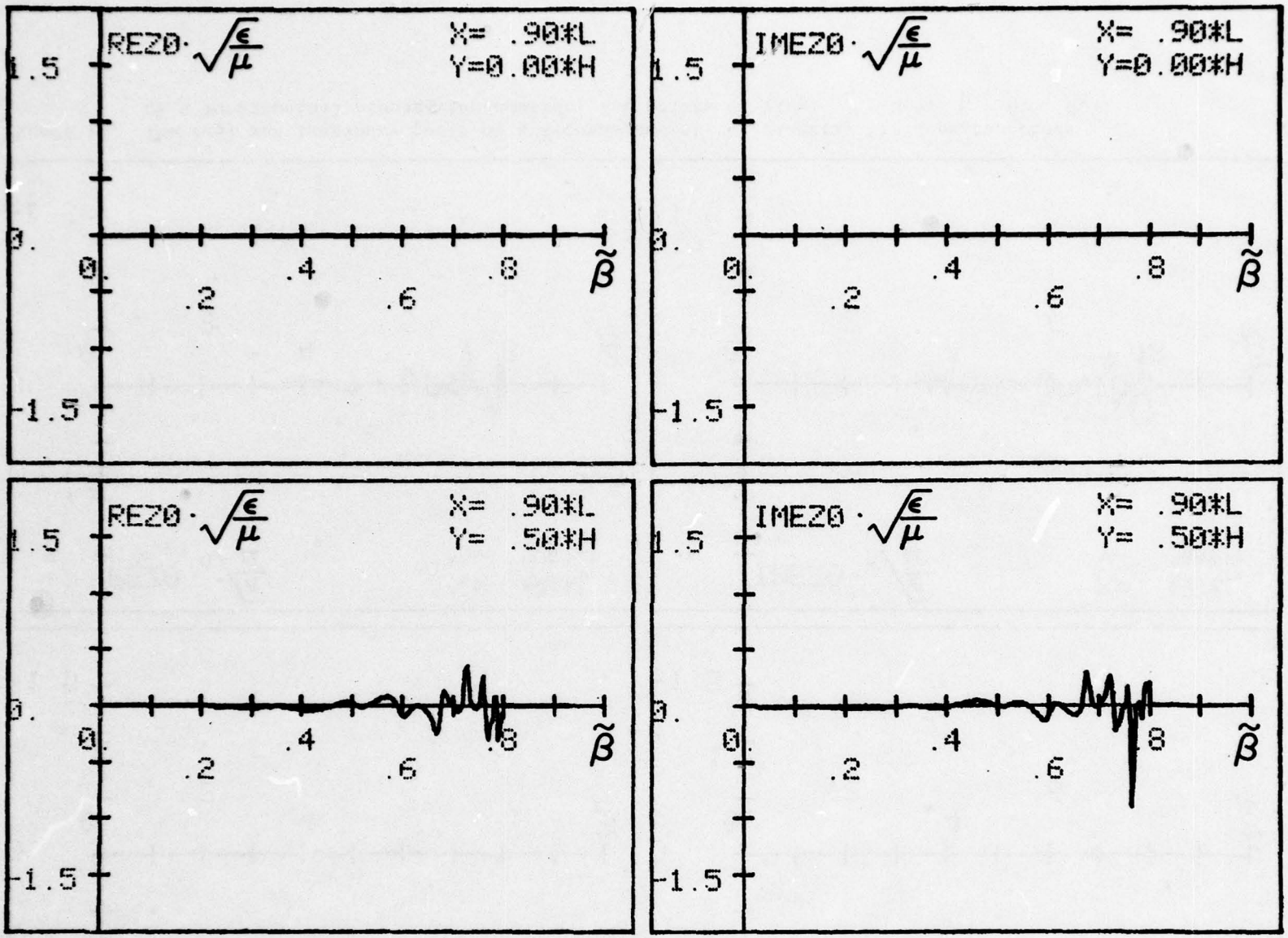

Figure 13. The real and imaginary parts of a z-component of the electric field as functions of a longitudinal propagation constant for points of view: $\frac{X}{L} = 0.9$; $\frac{Y}{H} = 0.0, 0.5$.

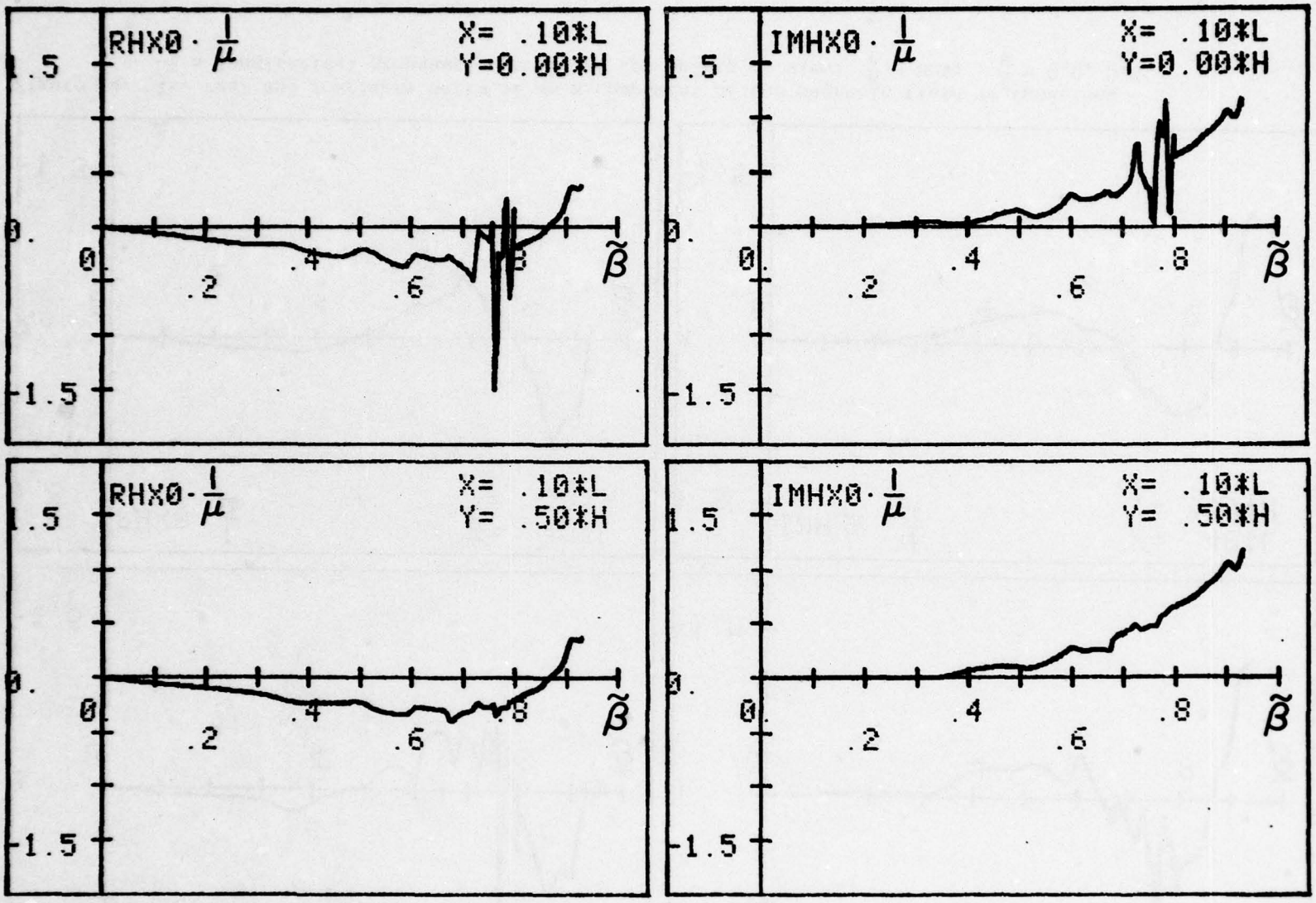

Figure 14. The real and imaginary parts of an x-component of the magnetic field as functions of a longitudinal propagation constant for points of view: $\frac{x}{L} = 0.1$; $\frac{Y}{H} = 0.0, 0.5$.

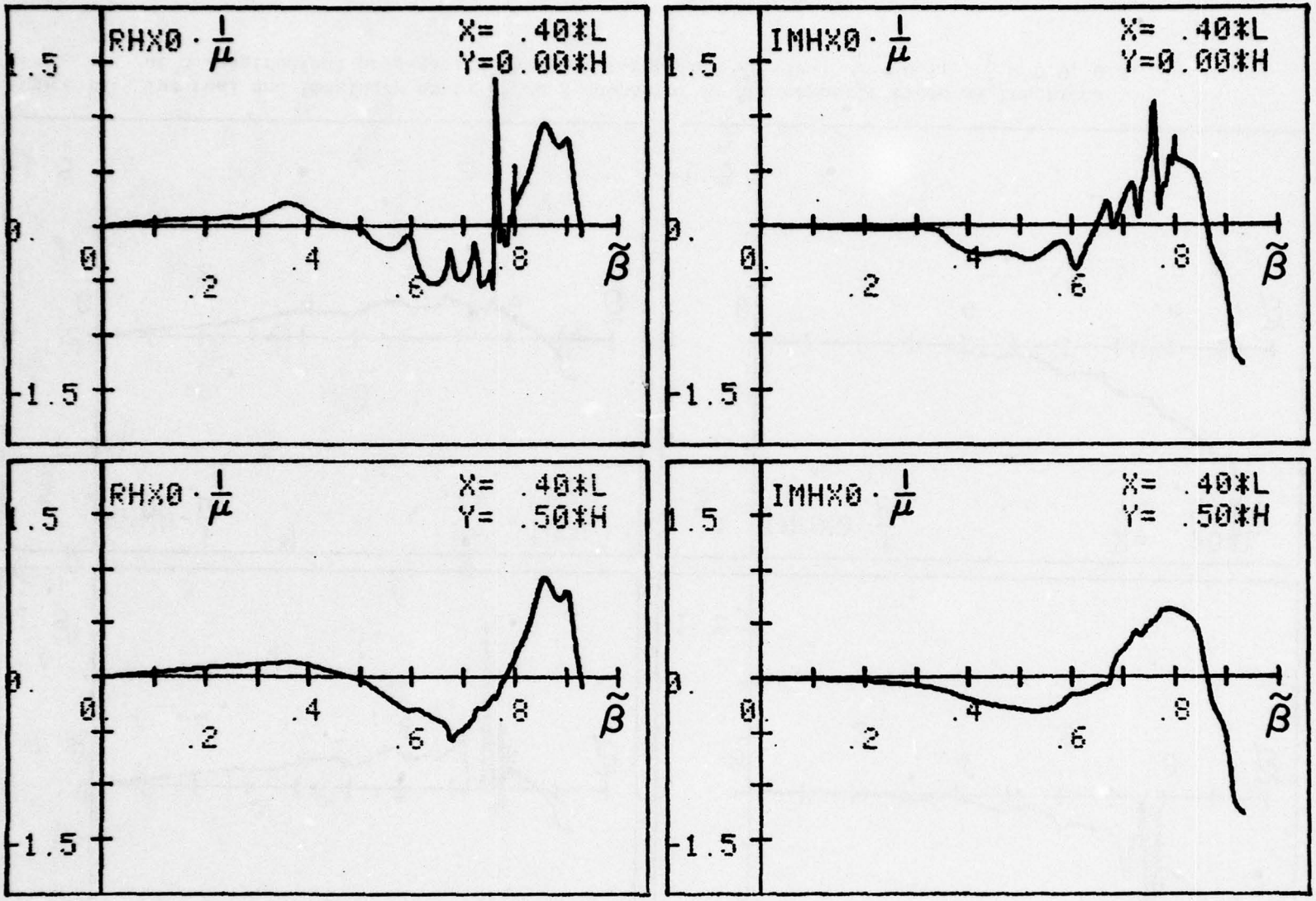

Figure 15. The real and imaginary parts of an x-component of the magnetic field as functions of a longitudinal propagation constant for points of view: $\frac{x}{L} = 0.4$; $\frac{y}{H} = 0.0, 0.5$.

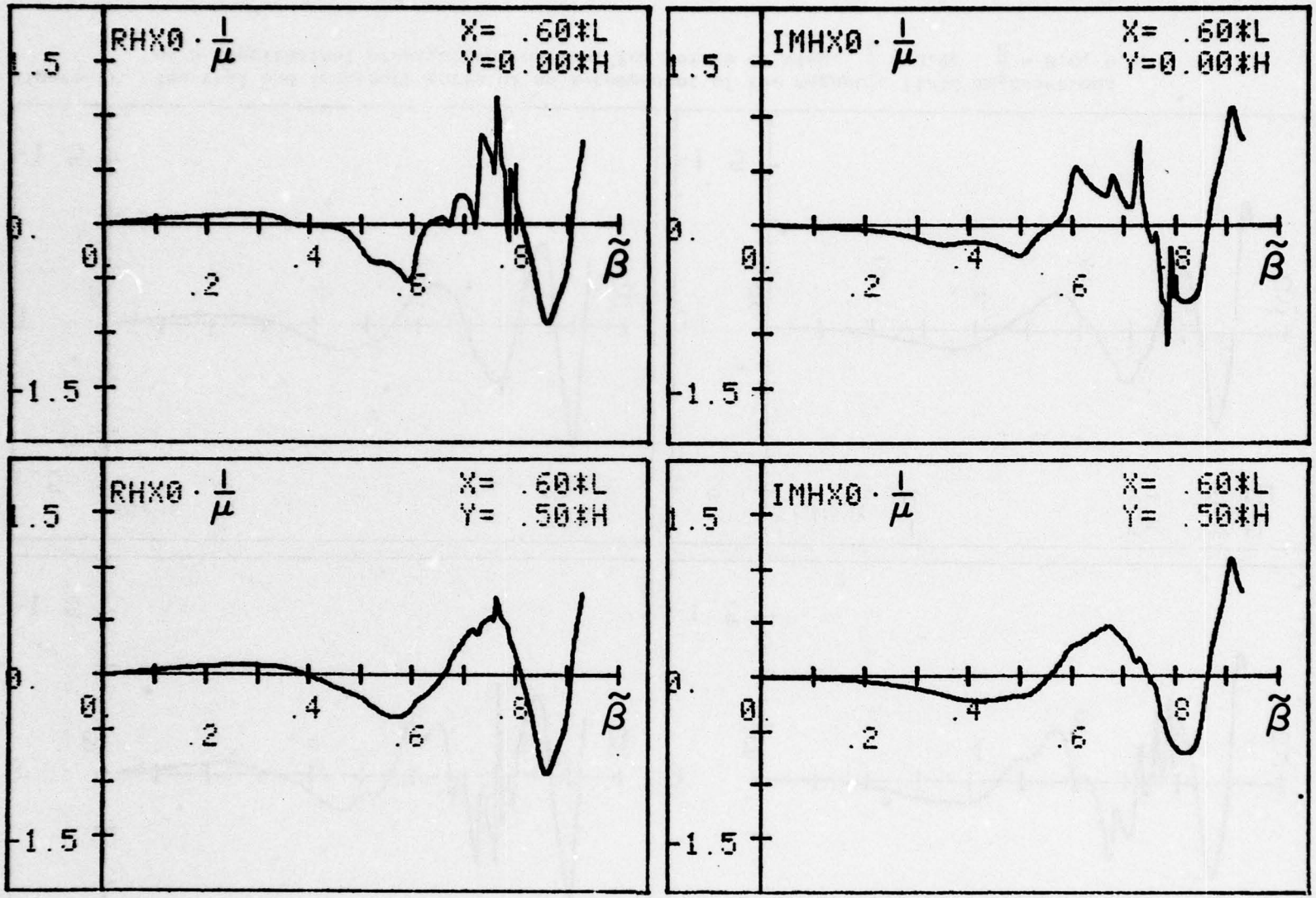

Figure 16. The real and imaginary parts of an x-component of the magnetic field as functions of a longitudinal propagation constant for points of view: $\frac{X}{L} = 0.6$; $\frac{Y}{H} = 0.0, 0.5$.

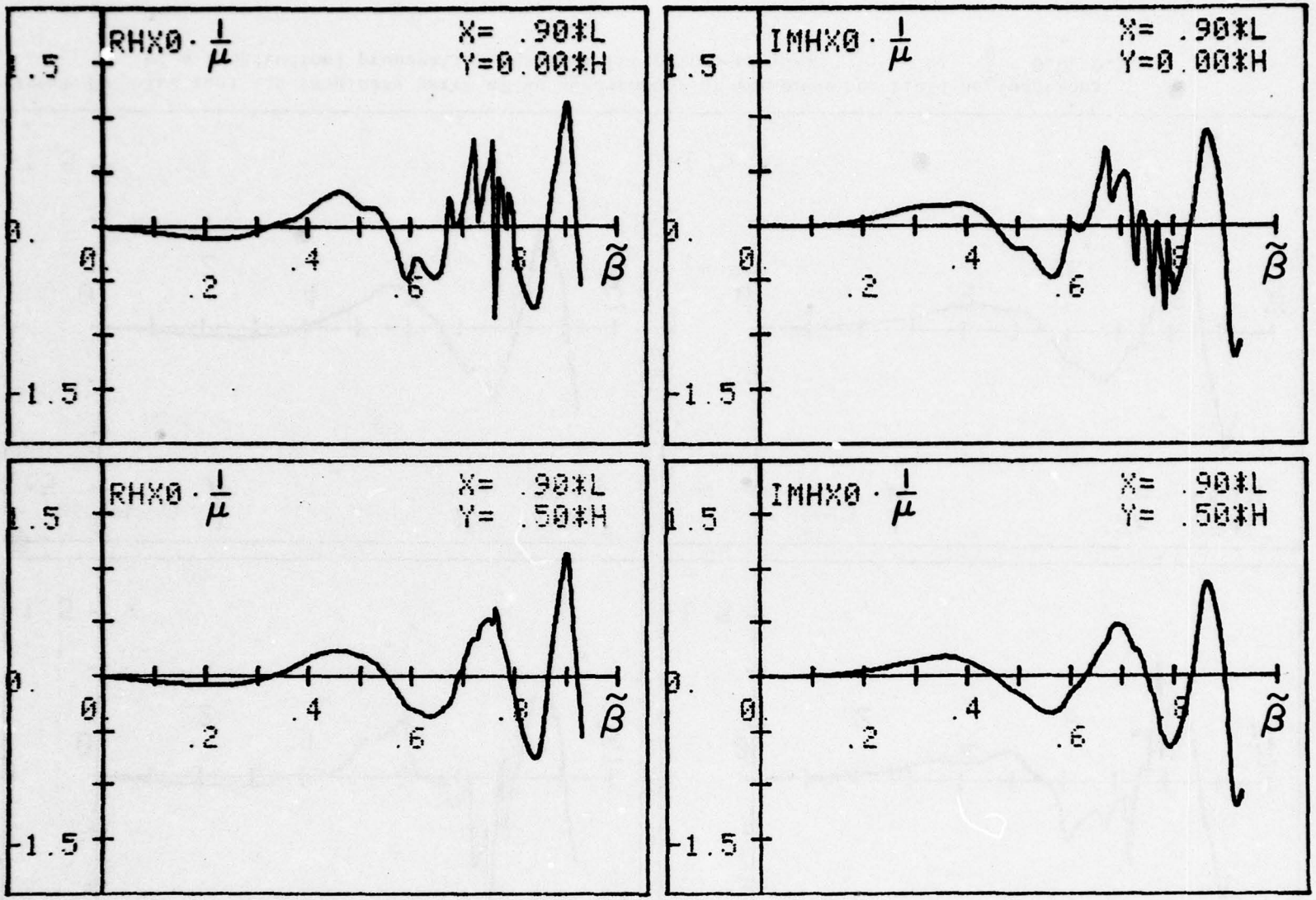

Figure 17. The real and imaginary parts of an x-component of the magnetic field as functions of a longitudinal propagation constant for points of view: $\frac{x}{L} = 0.9$; $\frac{Y}{H} = 0.0, 0.5$.

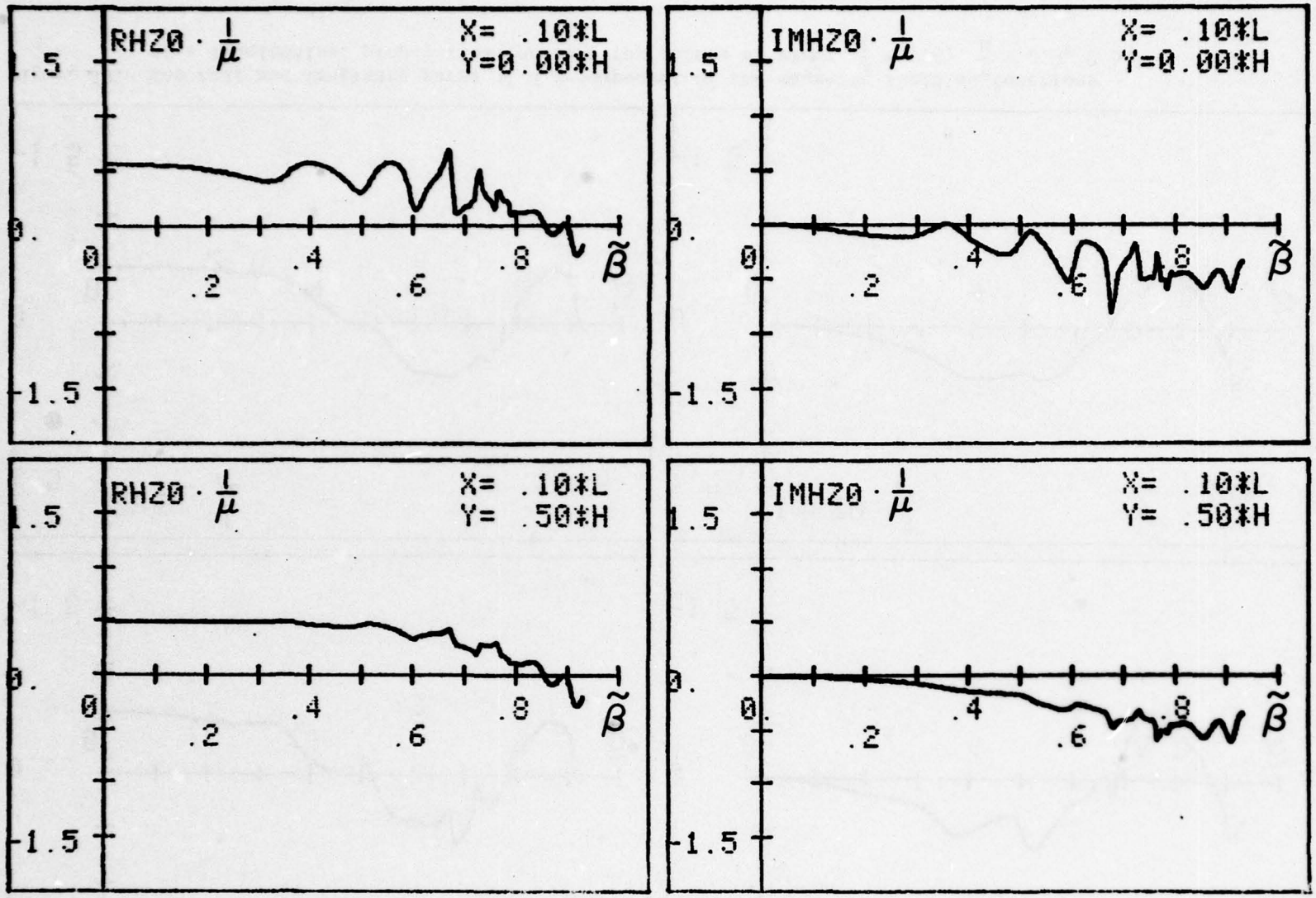

Figure 18. The real and imaginary parts of a z-component of the magnetic field as functions of a longitudinal propagation constant for points of view: $\frac{x}{L} = 0.1$; $\frac{Y}{H} = 0.0, 0.5$.

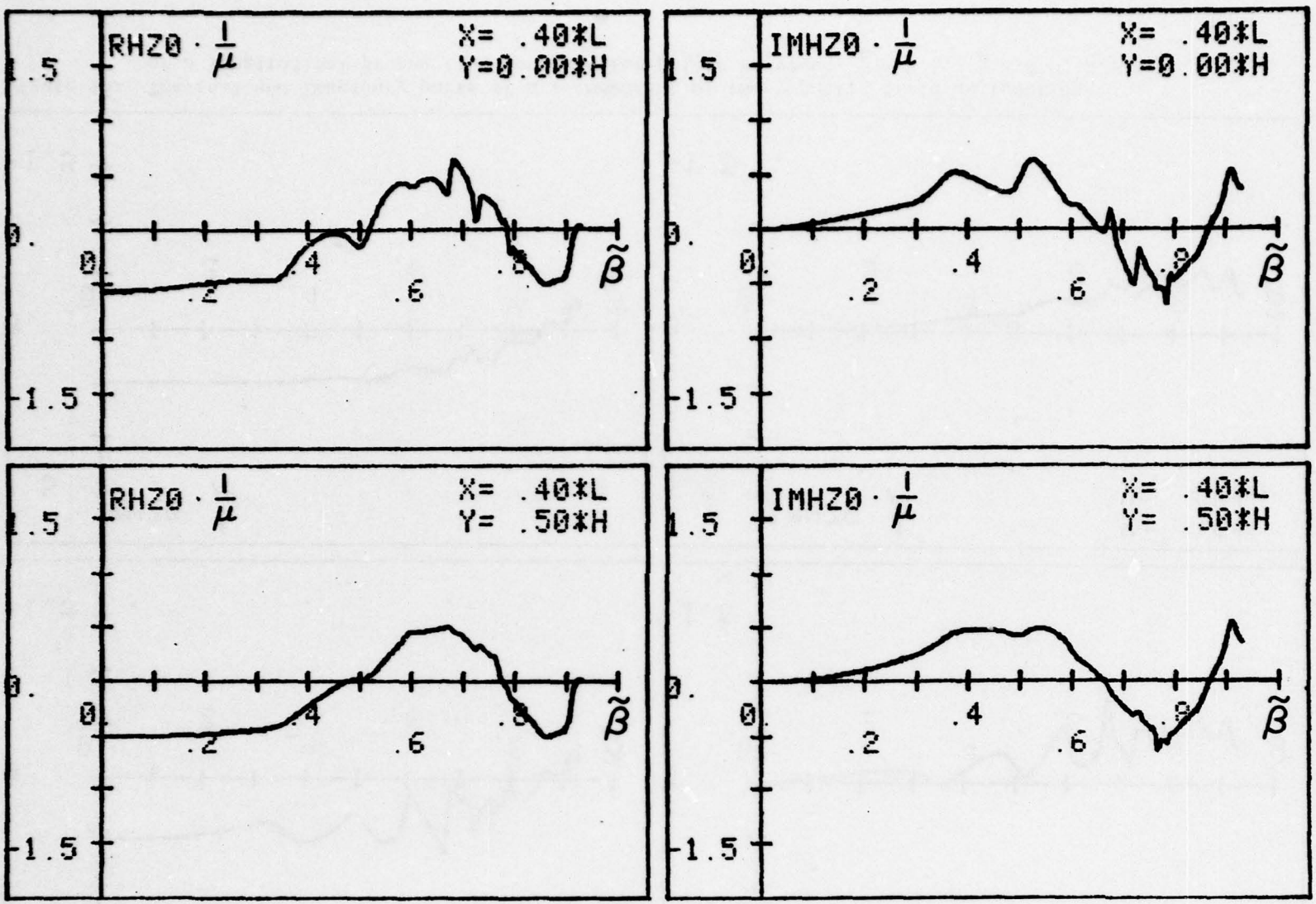

Figure 19. The real and imaginary parts of a z-component of the magnetic field as functions of a longitudinal propagation constant for points of view: $\frac{X}{L} = 0.4$; $\frac{Y}{H} = 0.0, 0.5$.

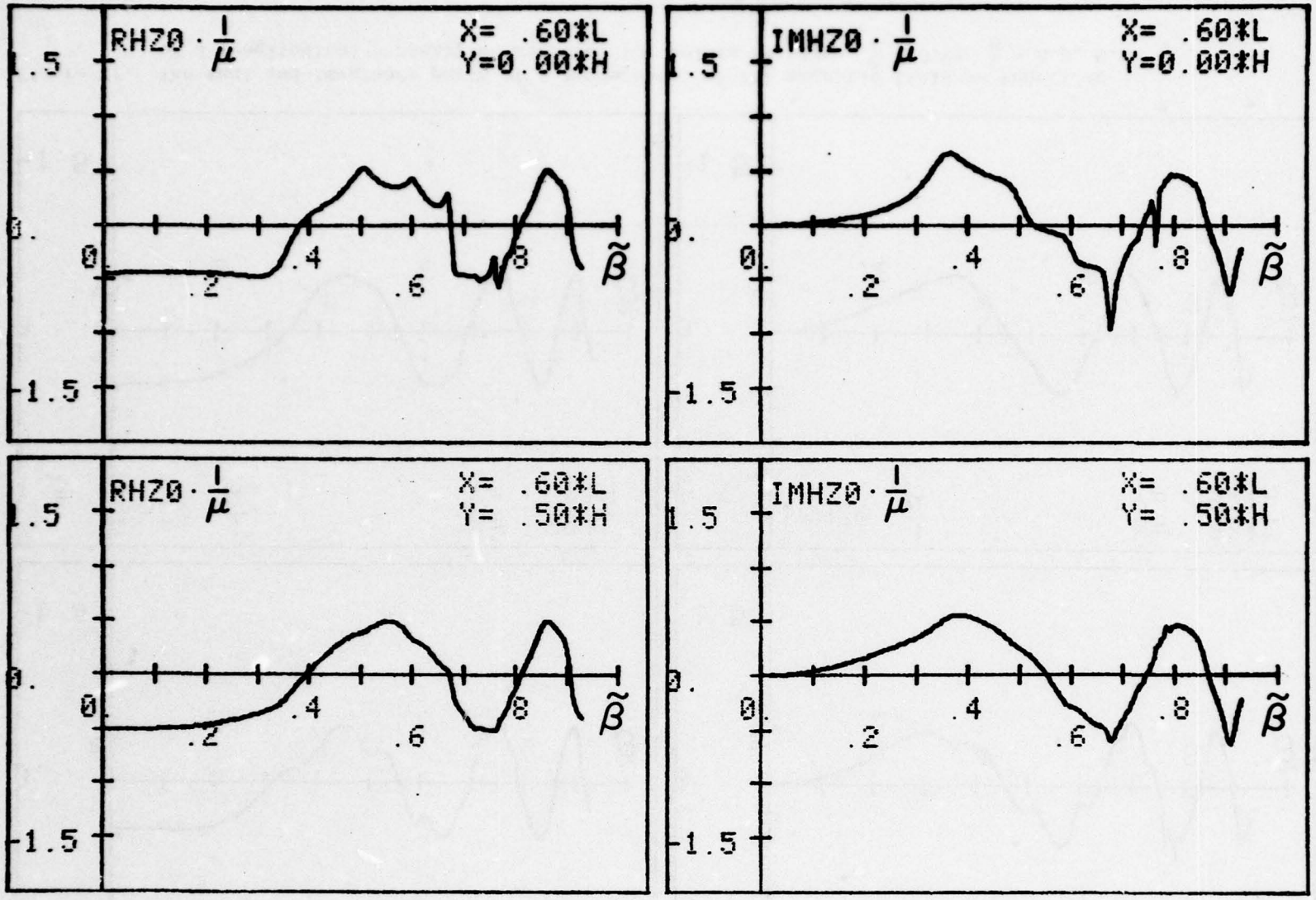

Figure 20. The real and imaginary parts of a z-component of the magnetic field as functions of a longitudinal propagation constant for points of view: $\frac{x}{L} = 0.6$; $\frac{Y}{H} = 0.0, 0.5$.

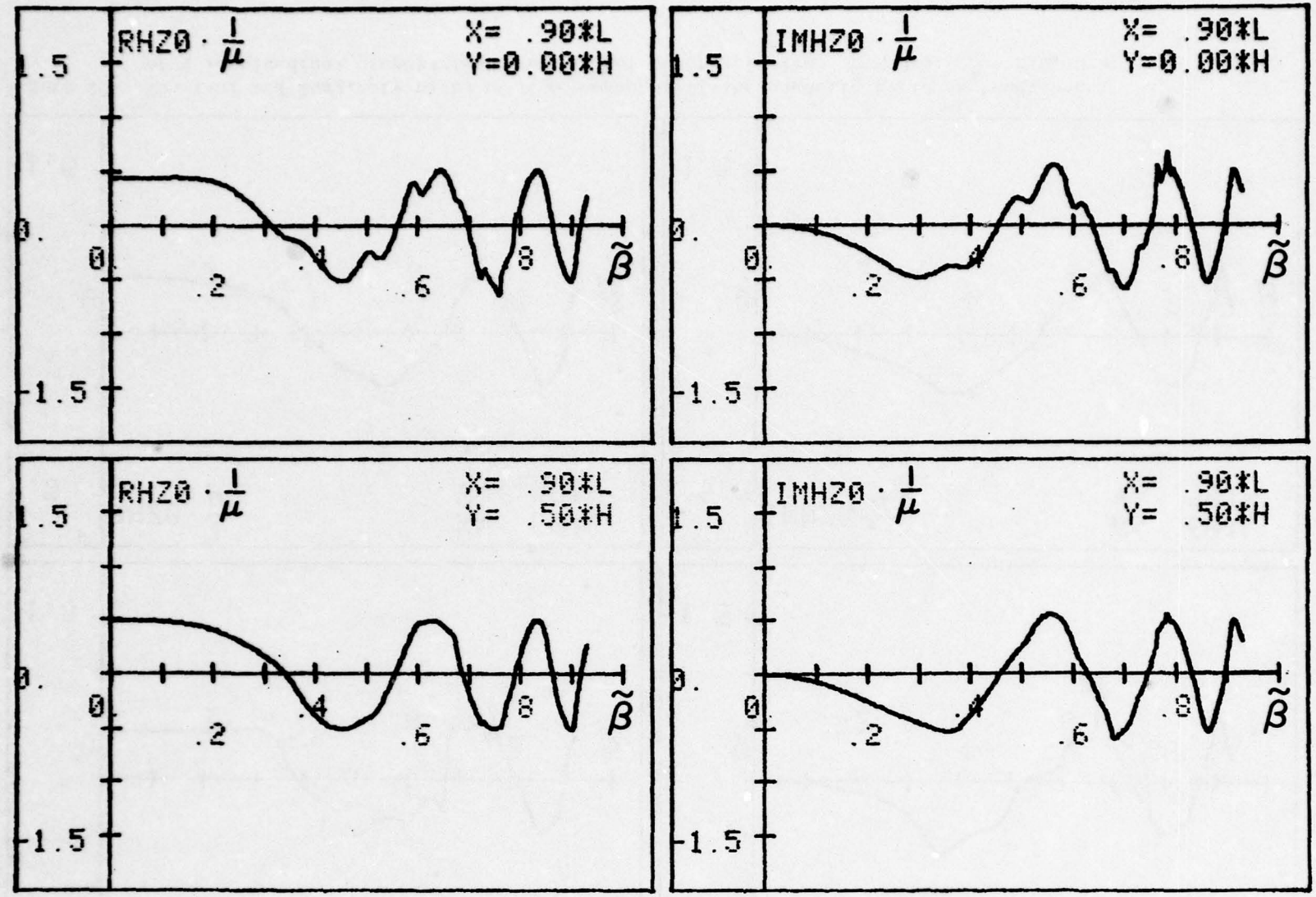

Figure 21. The real and imaginary parts of a z-component of the magnetic field as functions of a longitudinal propagation constant for points of view: $\frac{X}{L} = 0.9$; $\frac{Y}{H} = 0.0, 0.5$.

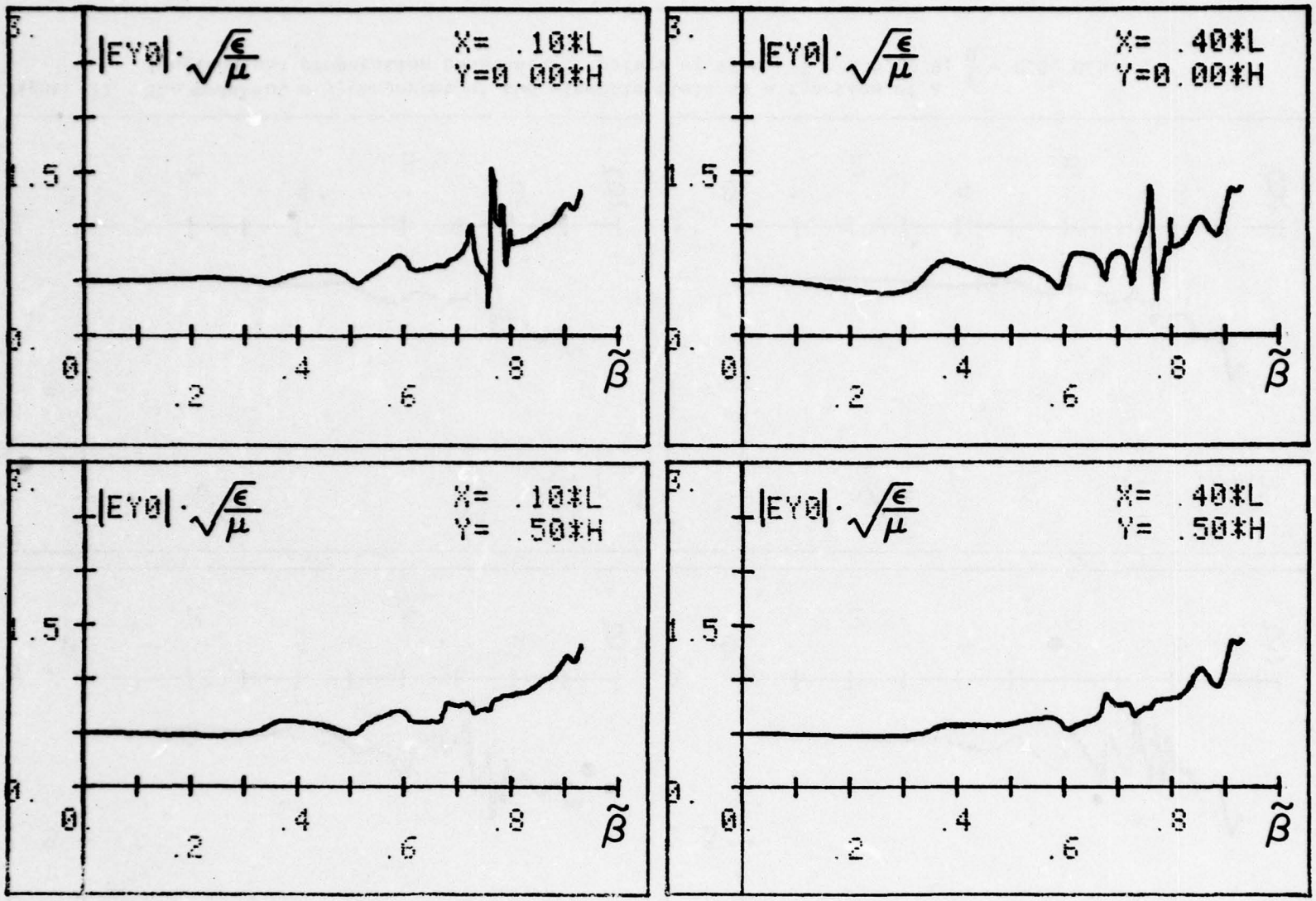

Figure 22. The module of a y-component of the electric field as a function of a longitudinal propagation constant for points of view: $\frac{x}{L}$ = 0.1, 0.4; $\frac{Y}{H}$ = 0.0, 0.5.

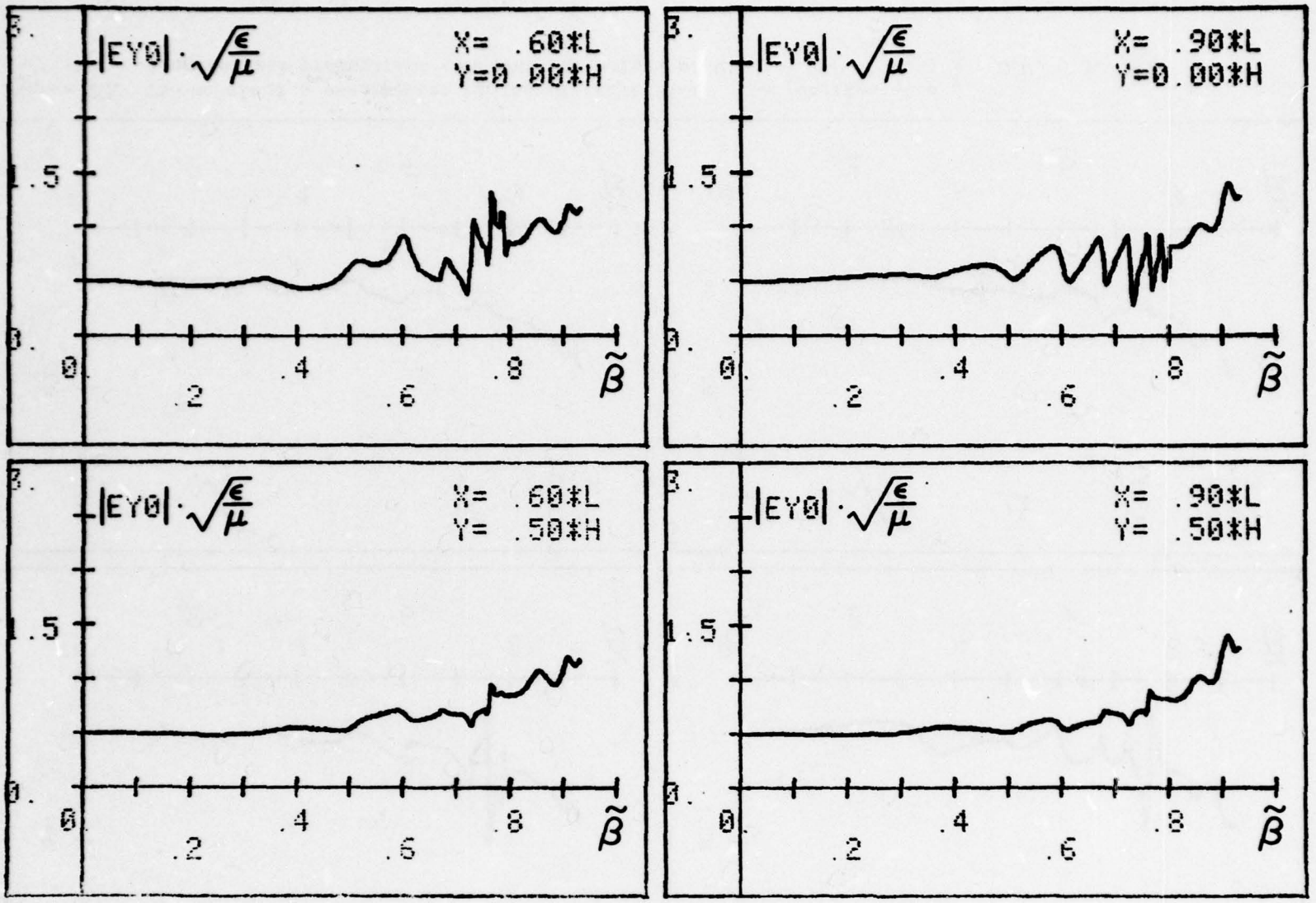

Figure 23. The module of a y-component of the electric field as a function of a longitudinal propagation constant for points of view: $\frac{X}{L}$ = 0.6, 0.9; $\frac{Y}{H}$ = 0.0, 0.5.

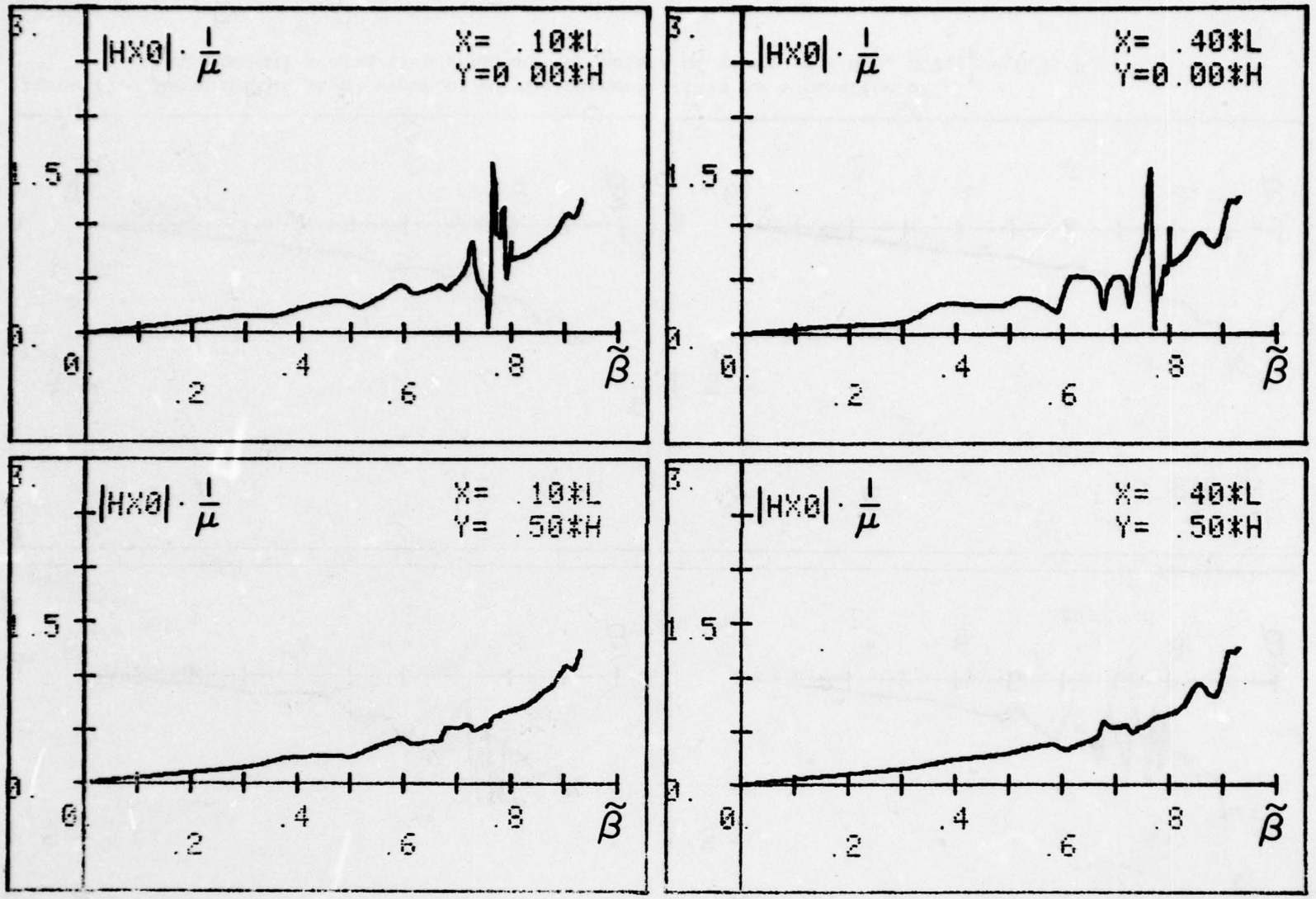

Figure 24. The module of an x-component of the magnetic field as a function of a longitudinal propagation constant for points of view: $\frac{X}{L}$ = 0.1, 0.4; $\frac{Y}{H}$ = 0.0, 0.5.

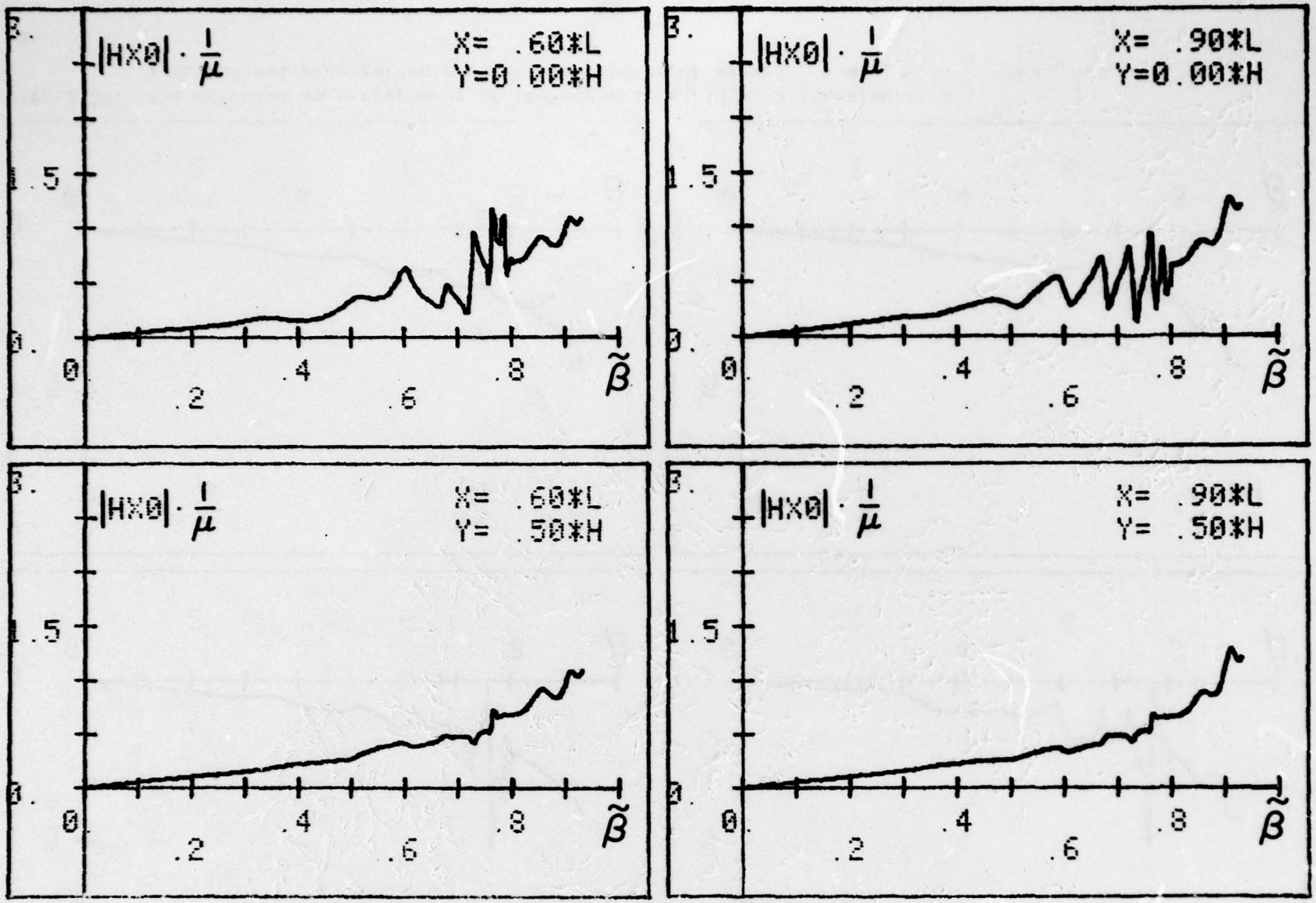

Figure 25. The module of an x-component of the magnetic field as a function of a longitudinal propagation constant for points of view: $\frac{X}{L}$ = 0.6, 0.9; $\frac{Y}{H}$ = 0.0, 0.5.

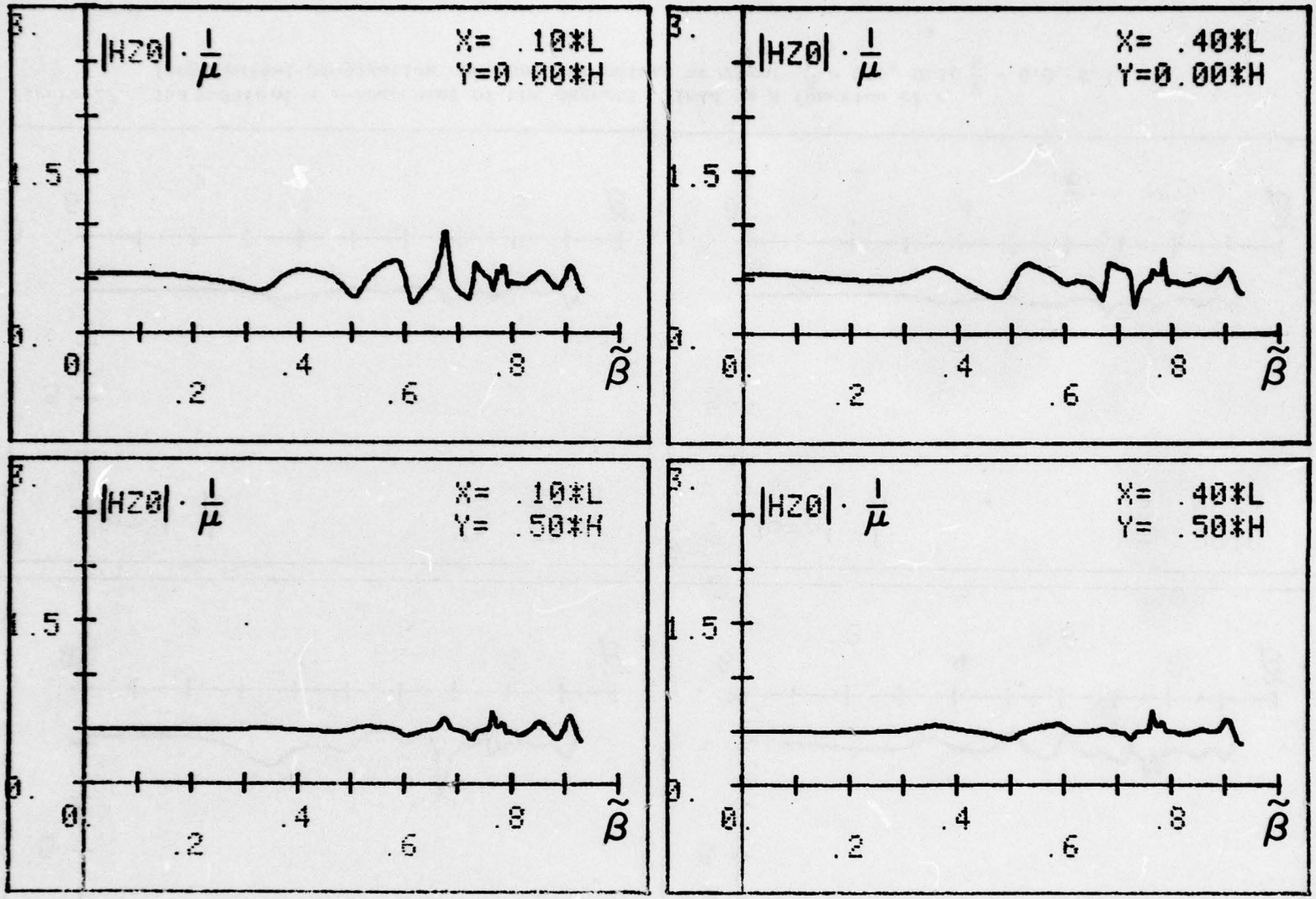

Figure 26. The module of a z-component of the magnetic field as a function of a longitudinal propagation constant for points of view: $\frac{X}{L}$ = 0.1, 0.4; $\frac{Y}{H}$ = 0.0, 0.5.

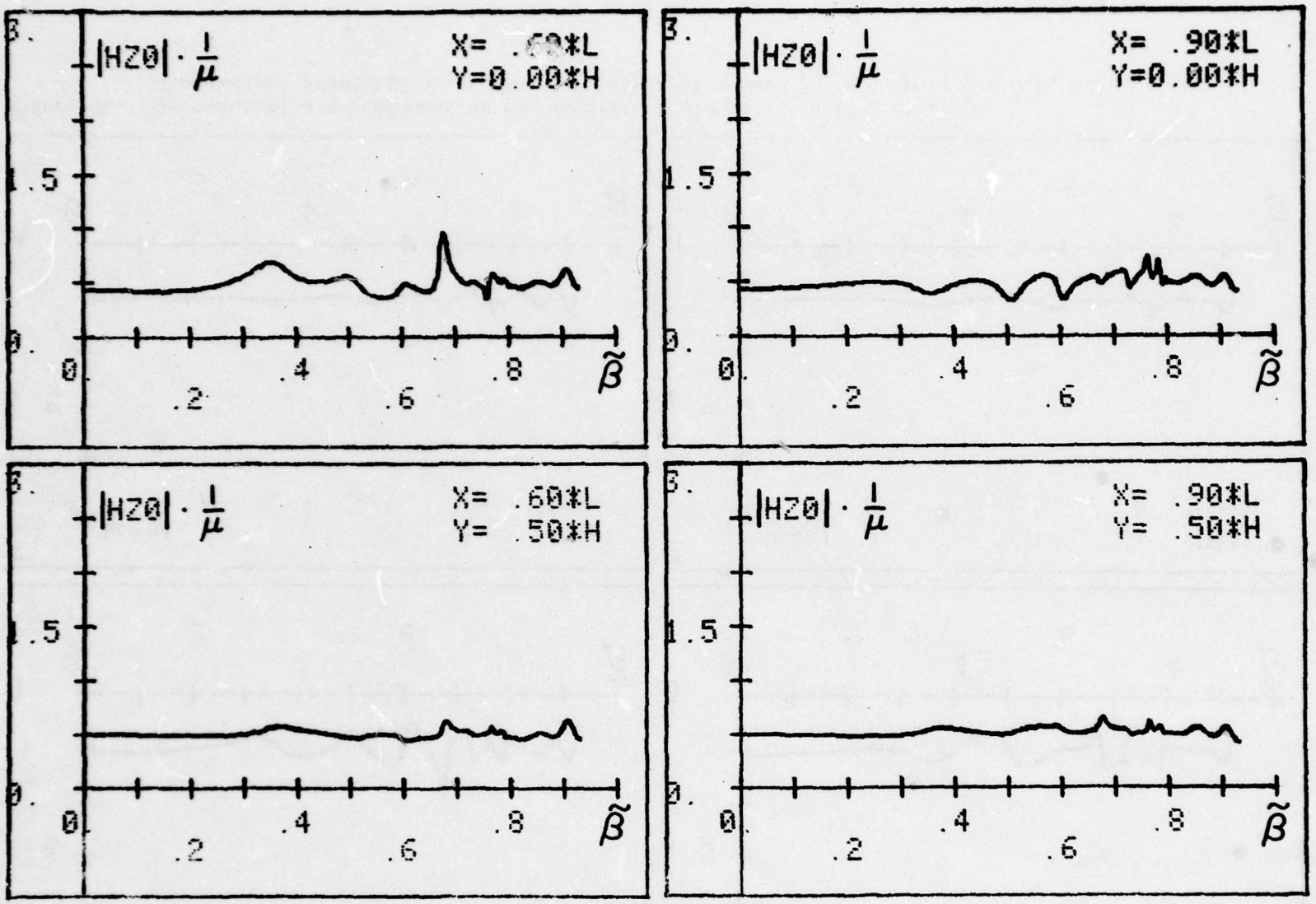

Figure 27. The module of a z-component of the magnetic field as a function of a longitudinal propagation constant for points of view: $\frac{X}{L}$ = 0.6, 0.9; $\frac{Y}{H}$ = 0.0, 0.5.

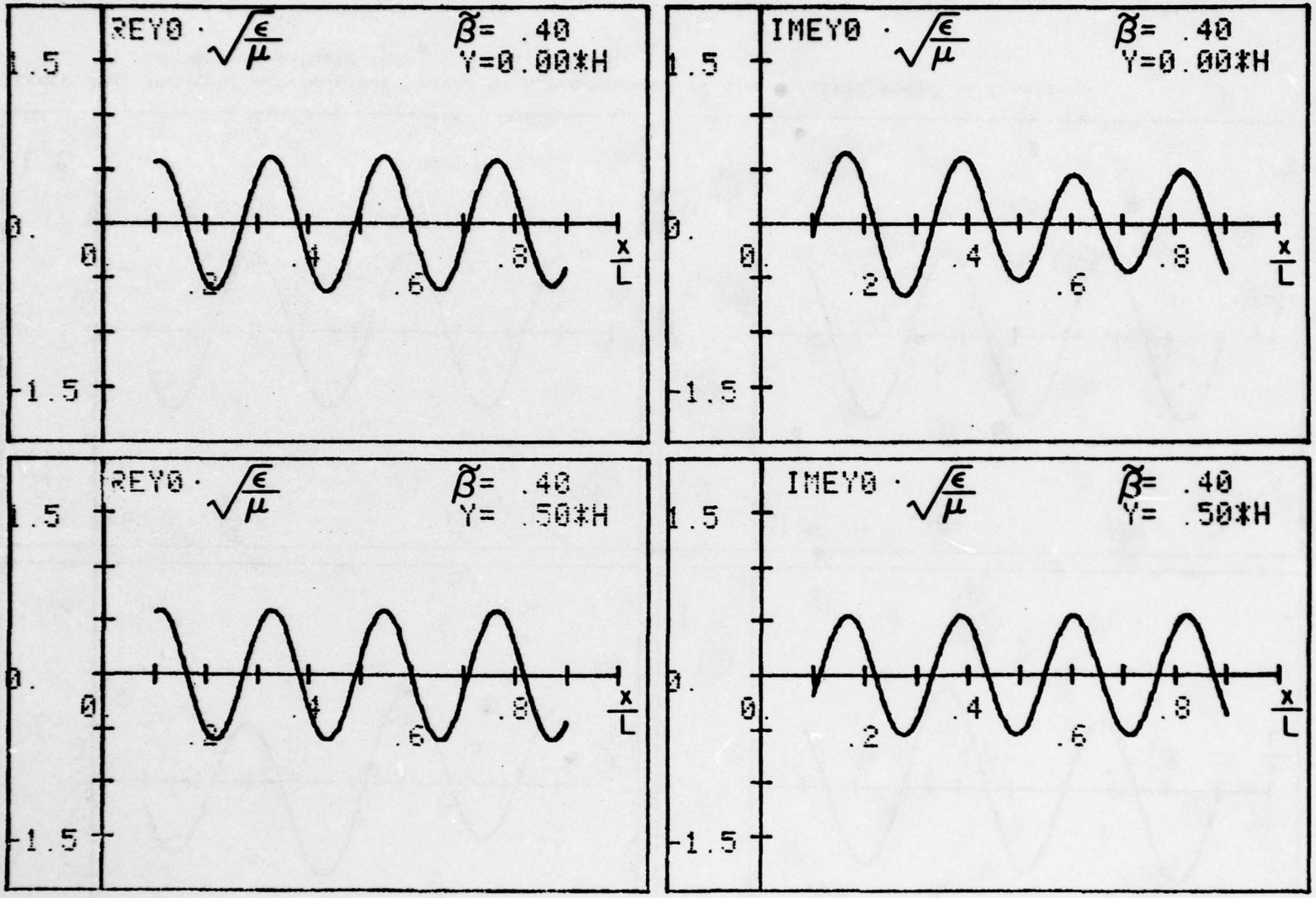

Figure 28. The real and imaginary parts of a y-component of the electric field as functions of an x-coordinate for $\tilde{\beta} = 0.4$; $\frac{Y}{H} = 0.0, 0.5$.

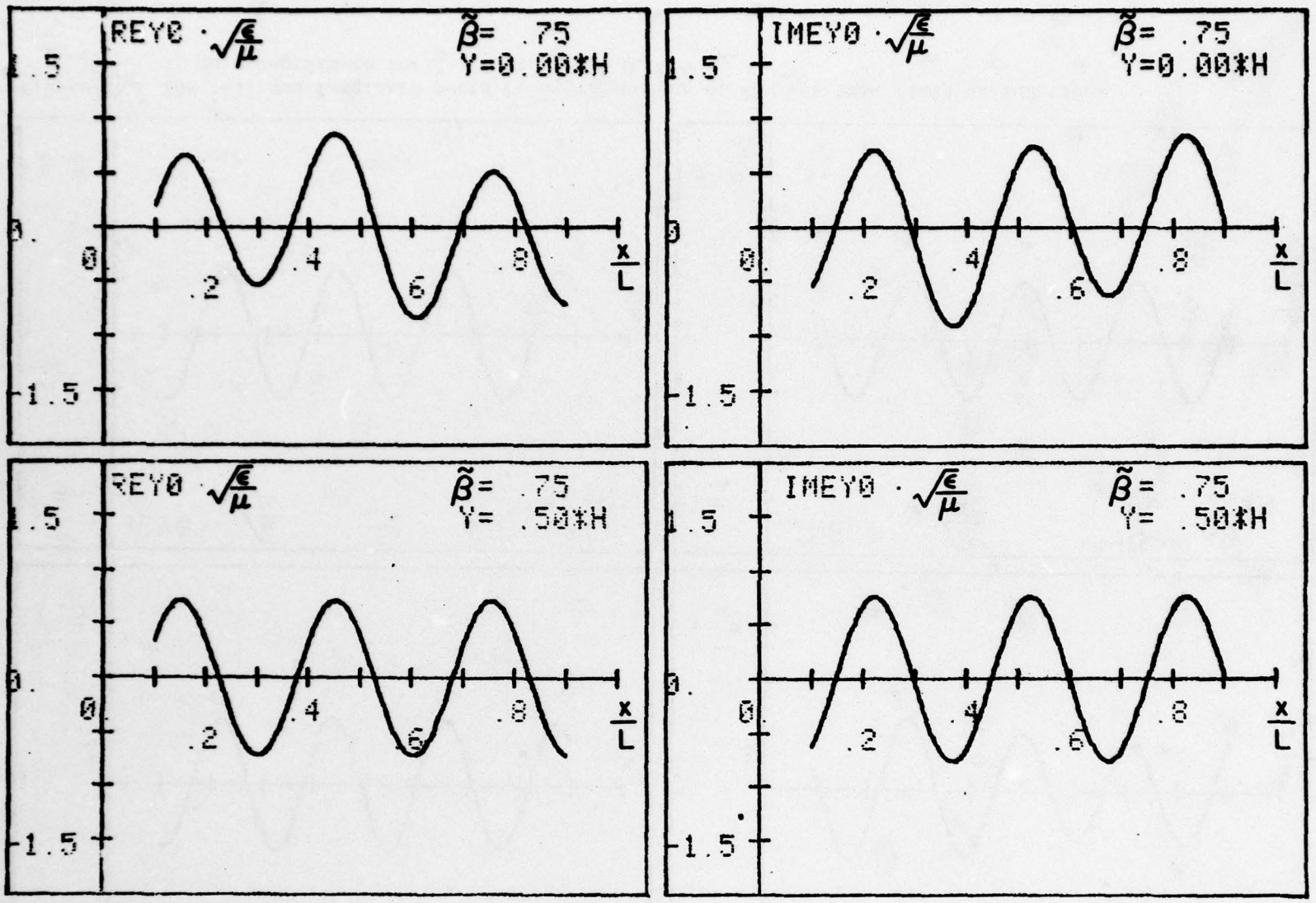

Figure 29. The real and imaginary parts of a $_y$-component of the electric field as functions of an x-coordinate for $\tilde{\beta}$ = 0.75; $\frac{Y}{H}$ = 0.0, 0.5.

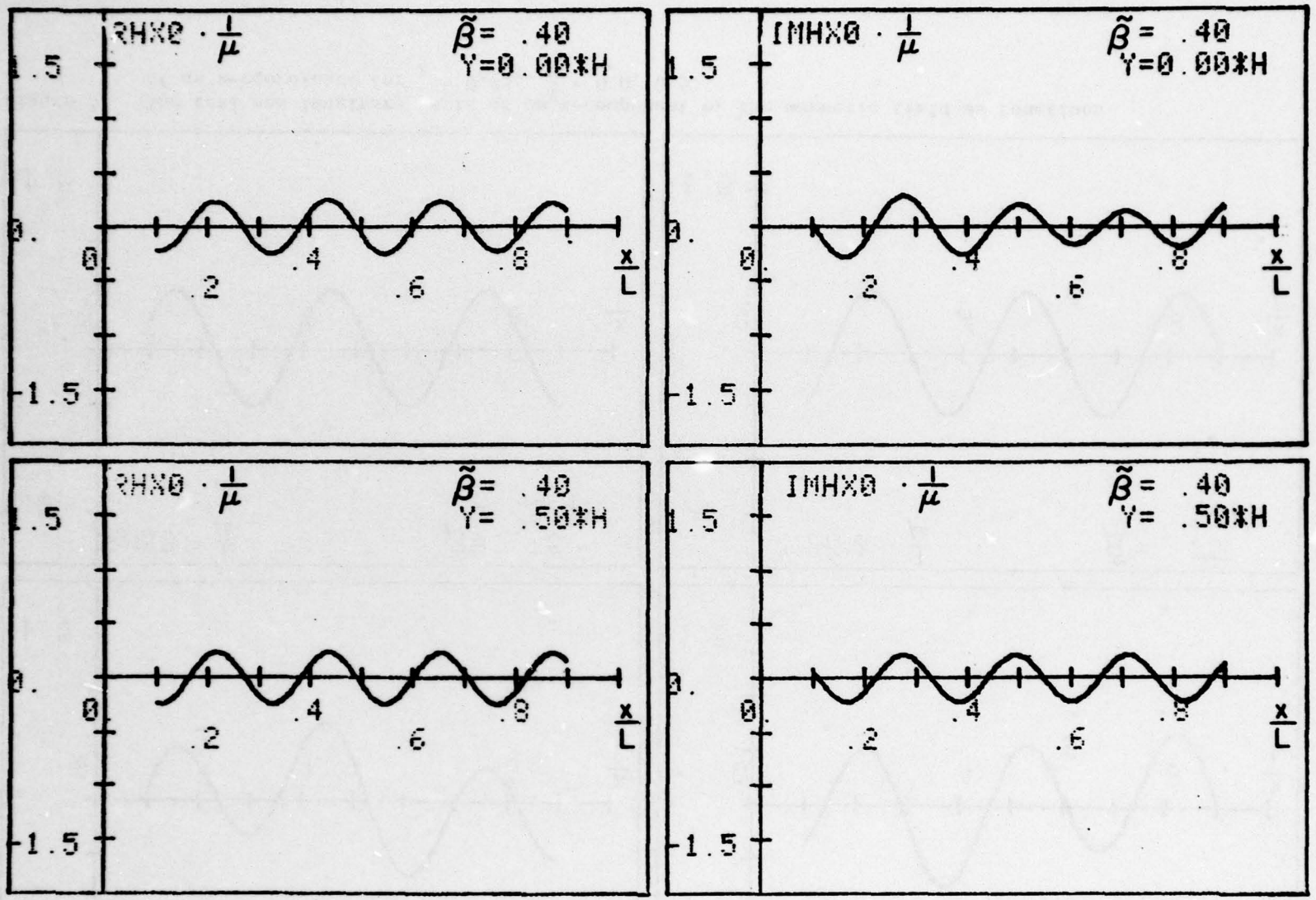

Figure 30. The real and imaginary parts of an x-component of the magnetic field as functions of an x-coordinate for $\tilde{\beta} = 0.4$; $\frac{Y}{H} = 0.0, 0.5$.

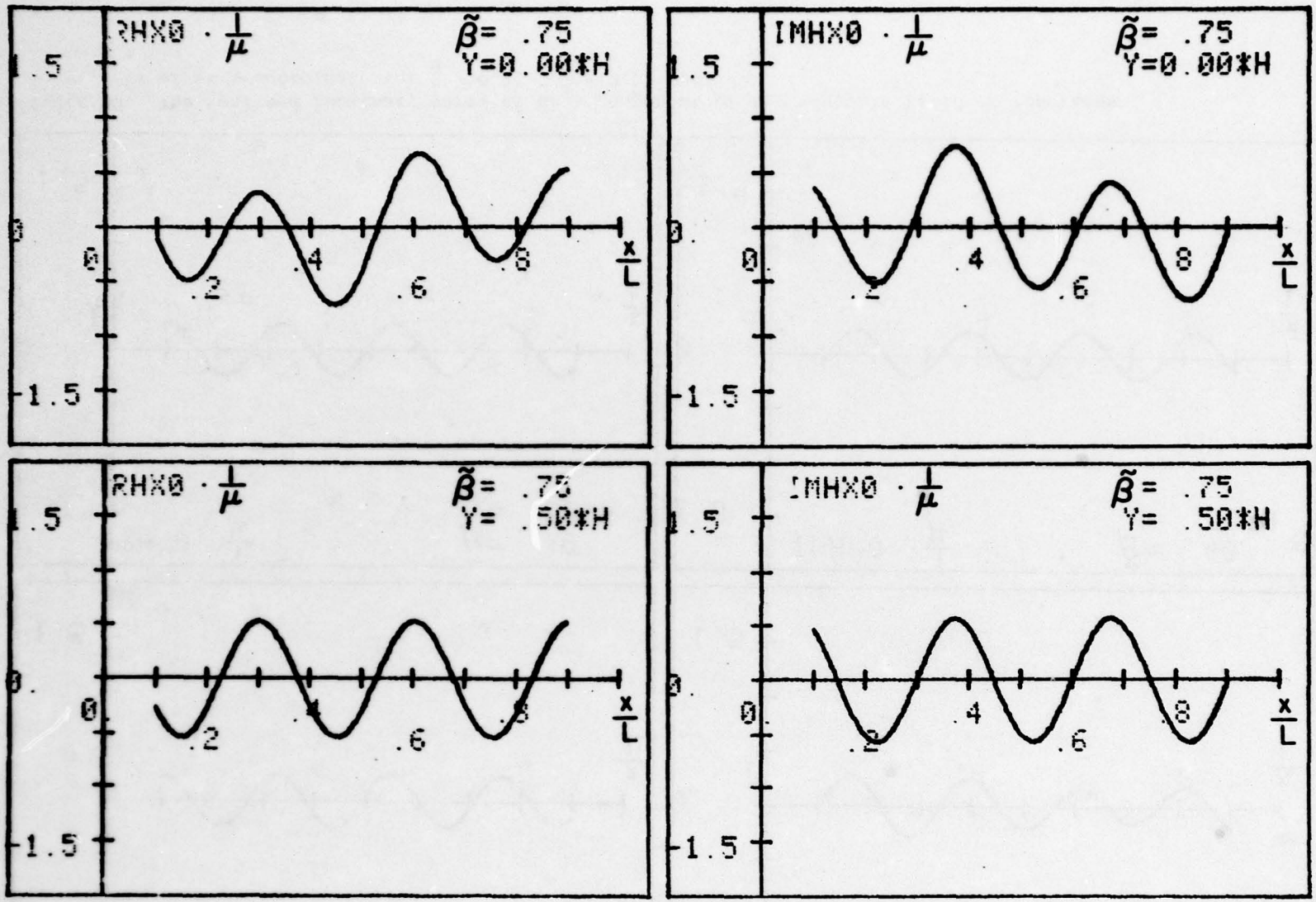

Figure 31. The real and imaginary parts of an x-component of the magnetic field as functions of an x-coordinate for $\tilde{\beta} = 0.75$; $\frac{Y}{H} = 0.0, 0.5$.

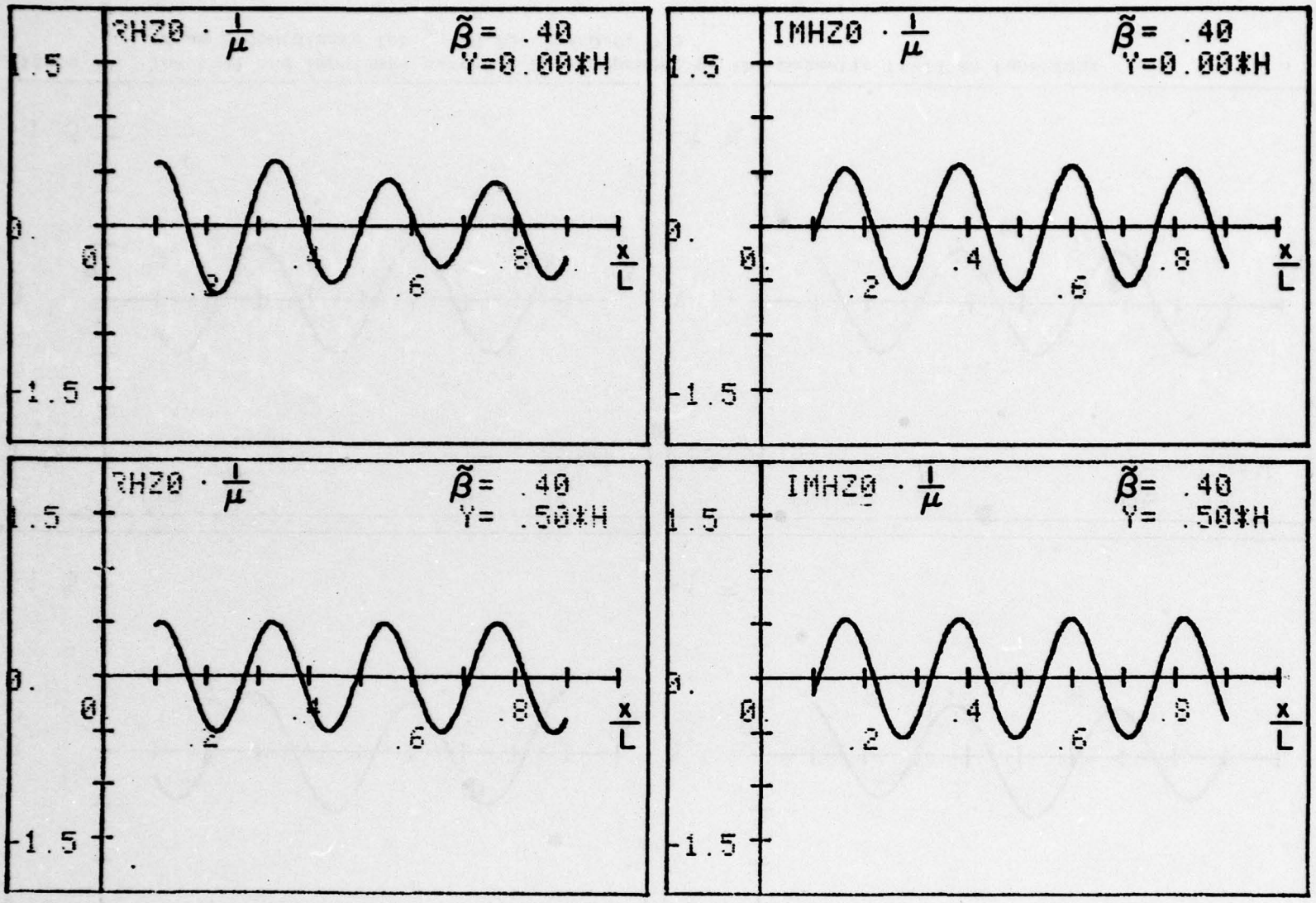

Figure 32. The real and imaginary parts of a A_z-component of the magnetic field as functions of an x-coordinate for $\tilde{\beta} = 0.4$; $\frac{Y}{H} = 0.0, 0.5$.

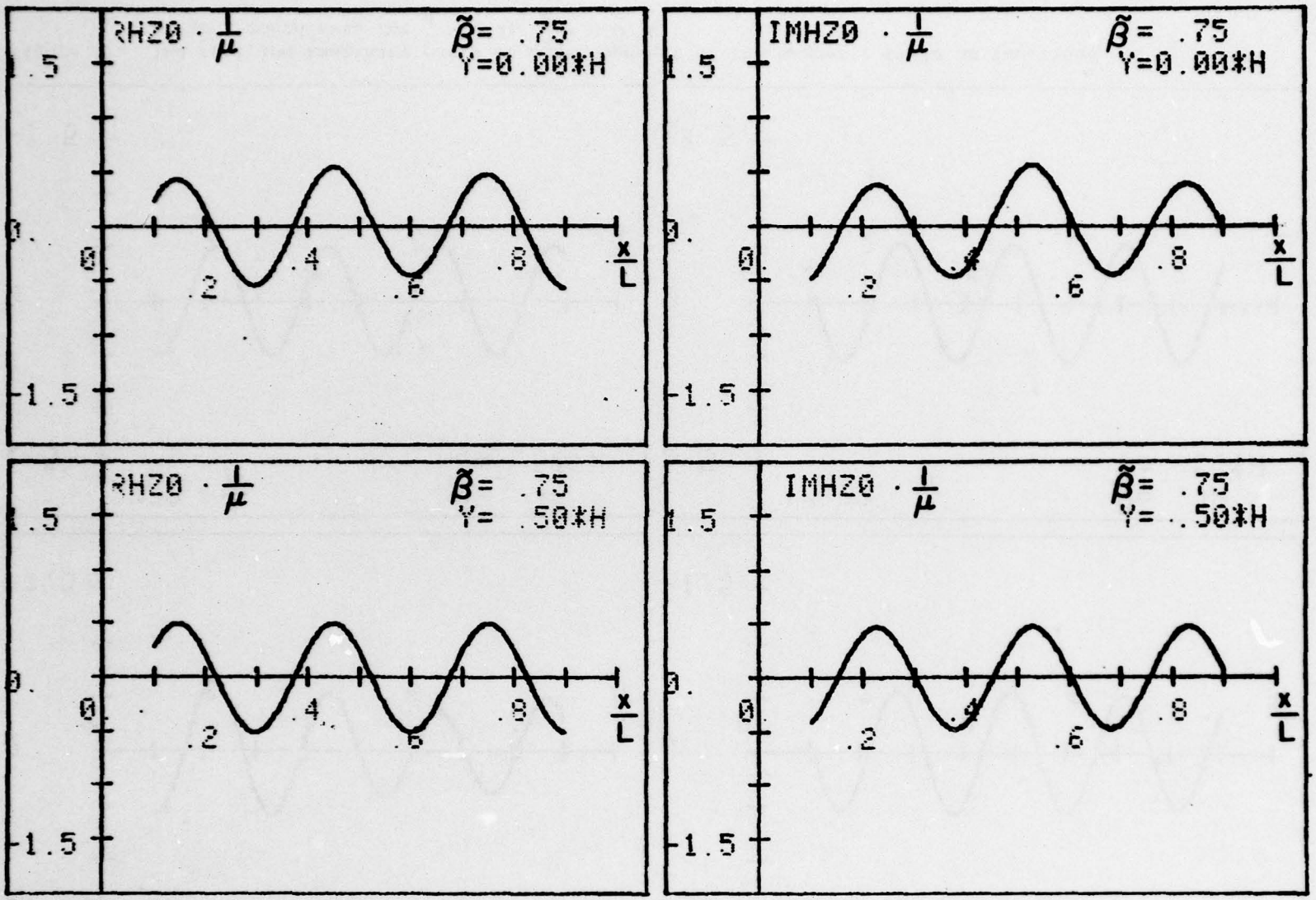

Figure 33. The real and imaginary parts of a_y z-component of the magnetic field as functions of an x-coordinate for $\tilde{\beta} = 0.75$; $\frac{Y}{H} = 0.0, 0.5$.

III. NUMERICAL STUDY OF THE PROBLEM

Because the analytical expressions derived in the second section are rather complicated and difficult to analyze, we numerically evaluated the solutions using a digital computer. The results are presented in this section in graphical form. This section consists of two parts: in the first we discuss the field components as functions of the longitudinal propagation constant; in the second - as functions of the transverse coordinates.

A. Real and Imaginary Parts and Amplitudes of the Field Components As Functions of the Longitudinal Propagation Constant

The graphics that are supplied in this section were plotted with a step for $\tilde{\beta}$ equal to 0.005. The point, $\tilde{\beta} = 0.80009$, also was used. The figures were plotted using 188 points. The output for the real and imaginary parts and the amplitudes of all five field components for eight observation points: $\frac{x}{L} = 0.1, 0.4, 0.6, 0.9$ and $\frac{Y}{H} = 0.0, 0.5$ are presented. From the figures it is observed that E_y, H_x, H_z are dominant components. In Figures 6-9 the real and imaginary parts of E_y are given. By comparing these results, one can observe for points $\frac{Y}{H} = 0.0$ and $\frac{Y}{H} = 0.5$ that the E_y, H_x, H_z - field behaviors as functions of $\tilde{\beta}$ are more complicated in the middle of the waveguide. This is hardly surprising in view of the largest contribution of the second mode for the above-mentioned components for $\frac{Y}{H} = 0.0$. When the point of observation approaches $\frac{Y}{H} = 0.5$, the contribution of the second mode for those components decreases and has a limiting value equal to zero. In Figures 6-9, 14-17, 22-25 we observe the step changing for the E_y, H_x components at $\tilde{\beta} = \tilde{\beta}_0$. The

second mode is responsible for this misbehavior. When $\frac{y}{H} \to 0.5$, the contribution of that step decreases, and for $\frac{y}{H} = 0.5$, it equals zero. One can observe that the curves are smooth at $\tilde{\beta} = \tilde{\beta}_0$. It should be mentioned that:

(a) The discontinuous behavior is observed because we have neglected the exponentially decreasing terms;

(b) In a lossy medium, the rate of decrease would be less. The H_z-component (see Figures 18-21, 26) doesn't have the step behavior because the contribution of the second mode is proportional to α_1, which goes to 0, when $\tilde{\beta} \to \tilde{\beta}_0$. The other two components, E_x and E_z, are equal to zero on the x-axis and have their largest contribution for $\frac{y}{H} = 0.5$ (see Figures 2-5, 10-13). E_x is smooth and E_z exhibits the step behavior at $\tilde{\beta}_0$. The figures demonstrate that the complexity of the curves occurs approximately in the region $0.7 < \tilde{\beta} < 0.8$, where we observe a sharp peak, which is due to the resonance. In the region $0 < \tilde{\beta} < 0.5$ the figures demonstrate the very smooth character of the curves.

B. Real and Imaginary Parts of the Field Components as Functions of Transverse Coordinates

In this section we present the real and imaginary parts of the dominant field components E_y, H_x, H_z as functions of the x-coordinate for two values of $\frac{y}{H} = 0.0$; 0.5 and two values of $\tilde{\beta} = 0.4$; 0.75. The graphic output, shown in Figures 28-33, was obtained using the results of calculations for 81 points of $\frac{x}{L}$ in the region [0.1, 0.9] (step = 0.010). All the graphs have very smooth characteristics. For $\tilde{\beta} = 0.75$ they have slightly more complicated form than for $\tilde{\beta} = 0.4$. As mentioned in the

previous section, for $\frac{y}{H} = 0.5$ the contribution of the second mode equals zero. We see that the amplitudes of the curves are constant for the entire region of view. For the $\frac{y}{H} = 0.0$, the field components are sums of the contributions of two modes. One can observe that the amplitudes of the curves are changing along the x-direction.

IV. CONCLUSIONS

In this report the problem of a source excitation of an open parallel-plate waveguide was developed. Extensive numerical results for the field components in the waveguide as functions of several parameters of the waveguide and propagation constant were supplied.

REFERENCES

[1] V. Krichevksy, R. Mittra, "Source Excitation of an Open, Parallel-Plate Waveguide," University of Illinois Electromagnetics Laboratory, Department of Electrical Engineering, Scientific Rep. No. 77-19, October 1977.

APPENDIX

SOURCE EXCITATION OF AN OPEN, PARALLEL-PLATE WAVEGUIDE PROGRAM

A complete program for source excitation of an open, parallel-plate waveguide program is presented. The computer program provides three-dimensional data-storage for the real and imaginary parts of five components of the EM field. Data were obtained for $\frac{x}{L}$ between 0.1 - 0.9 with step 0.1; $\frac{y}{H}$ between 0.0 - 0.9 with step 0.1; and $\tilde{\beta}$ - propagation constant between 0.0 - 0.93 with step 0.005 plus (•) 0.80009. These data were used to plot EM field components as functions of the propagation constant. The program can be readily modified to obtain data for plotting the EM-field component as a function of the x-coordinate.

```
      PROGRAM AFIELD(INPUT,OUTPUT,TAPE3,TAPE1=INPUT)
      COMPLEX BBK,BBAL,T1,F1,F2,EX0,EY0,EZ0,HX0,HZ0,CONST,AA,BB
      DIMENSION XX(9),YY(10),BETAB(188),REX0(10,9,188),AMEX0(10,9,188),
     $REY0(10,9,188),AMEY0(10,9,188),REZ0(10,9,188),AMEZ0(10,9,188),
     $RHX0(10,9,188),AMHX0(10,9,188),RHZ0(10,9,188),AMHZ0(10,9,188)
      READ(1,2)W,YBRI,YBRS,YBRF,XBRI,XBRS,XBRF
    2 FORMAT(F7.5,6(F7.3))
      M=1000
      PI=3.141592654
      CONST=CMPLX(0.,1.)
      CON=2.11593152
      BETAB(1)=0.
      DO 70 I=1,160
      BETAB(I+1)=BETAB(I)+0.005
   70 CONTINUE
      BETAB(162)=0.80009
      BETAB(163)=0.805
      DO 75 I=1,25
   75 BETAB(I+163)=BETAB(I+162)+0.005
      CONTINUE
      DO 98 N=1,161
      BETA=BETAB(N)
      K=N
      A=10.*PI*SQRT(1.-BETA**2)
      B=A*W/PI
      ALFA1=SQRT(B**2-1.)
      DD=PI*ALFA1/W
      CALL BE1(A,B,BBK,PI,M,CON,ALFA1)
      CALL BE2(A,B,BBAL,PI,M,CON,ALFA1)
      CALL TE1(A,B,T1,BBK,PI)
      CALL F12(A,B,T1,ALFA1,BBK,BBAL,F1,F2)
      X=XBRI
      J=1
   30 Y=YBRI
      I=1
   20 EX0=(PI*ALFA1/(10.*W**2))*F2*SIN(PI*Y)*SIN(DD*X)
      EY0=10.*PI*(F1*COS(A*X)+(1.-(1./(100.*W**2)))*F2*COS(PI*Y)*
     $COS(DD*X)-CEXP(CMPLX(0.,A*X))/(2.*A))
      EZ0=-CONST*BETA*(PI/W)*F2*SIN(PI*Y)*COS(DD*X)
      HX0=-BETA*10.*PI*(F1*COS(A*X)+F2*COS(PI*Y)*COS(DD*X)-(1./(2.*A))*
     $CEXP(CMPLX(0.,A*X)))
      HZ0=CONST*A*F1*SIN(A*X)+CONST*DD*F2*COS(PI*Y)*SIN(DD*X)-
     $0.5*CEXP(CMPLX(0.,A*X))
      REX0(I,J,K)=REAL(EX0)
      AMEX0(I,J,K)=AIMAG(EX0)
      REY0(I,J,K)=REAL(EY0)
```

```
      AMEY0(I,J,K)=AIMAG(EY0)
      REZ0(I,J,K)=REAL(EZ0)
      AMEZ0(I,J,K)=AIMAG(EZ0)
      RHX0(I,J,K)=REAL(HX0)
      AMHX0(I,J,K)=AIMAG(HX0)
      RHZ0(I,J,K)=REAL(HZ0)
      AMHZ0(I,J,K)=AIMAG(HZ0)
      Y=Y+YBRS
      I=I+1
      IF(Y.LE.YBRF) GO TO 20
      X=X+XBRS
      J=J+1
      IF(X.LE.XBRF) GO TO 30
   98 CONTINUE
      DO 99 L=162,188
      BETA=BETAB(L)
      K=L
      A=10.*PI*SQRT(1.-BETA**2)
      X=XBRI
      J=1
      B=A*W/PI
      CALL BE(A,B,BB,PI,M)
      X=XBRI
   17 AA=CEXP(CMPLX(0.,A*X))
      EY0=-0.5*(AA-BB*COS(A*X))/SQRT(1.-BETA**2)
      HX0=-BETA*EY0
      HZ0=0.5*(-SIGN(1.,X)*AA+CONST*BB*SIN(A*X))
      DO 18 I=1,10
      REX0(I,J,K)=0.
      AMEX0(I,J,K)=0.
      REZ0(I,J,K)=0.
      AMEZ0(I,J,K)=0.
      REY0(I,J,K)=REAL(EY0)
      AMEY0(I,J,K)=AIMAG(EY0)
      RHX0(I,J,K)=REAL(HX0)
      AMHX0(I,J,K)=AIMAG(HX0)
      RHZ0(I,J,K)=REAL(HZ0)
   18 AMHZ0(I,J,K)=AIMAG(HZ0)
      X=X+XBRS
      J=J+1
      IF(X.LE.XBRF) GO TO 17
   99 CONTINUE
      WRITE(3,101) REX0,AMEX0,REY0,AMEY0,REZ0,AMEZ0,RHX0,AMHX0,RHZ0,AM
     $HZ0
  101 FORMAT(10F8.5)
      DY=0.1
      DX=0.1
      YY(1)=0.
      DO 50 I=1,9
      YY(I+1)=YY(I)+DY
   50 CONTINUE
```

```
      XX(1)=0.1
      DO 60 I=1,8
      XX(I+1)=XX(I)+DX
   60 CONTINUE
      WRITE(3,101) YY,XX,BETAB
      STOP
      END
      SUBROUTINE BE1(A,B,BBK,PI,M,CON,ALFA1)
      COMPLEX F,BBK
      AM1=0.
      DO 10 I=2,M
      AM1=AM1+B/I-ASIN(B/I)
   10 CONTINUE
      F=CEXP(CMPLX(-B*PI/2.,B*(CON-ALOG(B))-PI/2.+A+AM1))
      BBK=(ALFA1+B)*F
      RETURN
      END
      SUBROUTINE BE2(A,B,BBAL,PI,M,CON,ALFA1)
      COMPLEX F,BBAL,D
      AM1=0.
      DO 10 I=2,M
      AM1=AM1+ALFA1/I-ASIN(ALFA1/SQRT(I**2-1.))
   10 CONTINUE
      F=CEXP(CMPLX(-ALFA1*PI/2.,ALFA1*(CON-ALOG(B))+AM1+ALFA1*A/B))
      D=CMPLX(1.,-ALFA1)
      BBAL=F*D*SQRT(2.)*ALFA1/B
      RETURN
      END
      SUBROUTINE TE1(A,B,T1,BBK,PI)
      COMPLEX T1,BBK,D1
      D=B*SQRT(PI)/SQRT(A*2.)
      D1=CMPLX(1.+D,-D)
      T1=BBK**2*D1
      RETURN
      END
      SUBROUTINE F12(A,B,T1,ALFA1,BBK,BBAL,F1,F2)
      COMPLEX T1,BBK,BBAL,F1,F2,D1
      D1=ALFA1*(1.+T1)*(BBAL**2*(4.*T1*B/(1.+T1)-(ALFA1+B)**2/ALFA1)/
     $(2.*ALFA1)-1.)
      F1=(BBK**2/((1.+T1)*A))*(1.+2.*B*BBAL**2/D1)
      F2=2.*B*BBK*BBAL/(A*D1)
      RETURN
      END
      SUBROUTINE BE(A,B,BB,PI,M)
      COMPLEX T,F,BB
      CONST=1.115931516
      AM1=0.
      DO 10 I=1,M
      AM1=AM1+B/I-ASIN(B/I)
   10 CONTINUE
      T=CEXP(CMPLX(-B*PI,2.*(B*(CONST-ALOG(B))+A+AM1)))
      F1=SQRT(PI)*B/SQRT(2.*A)
      F=CMPLX(1.+F1,-F1)
      BB=2.*T/(1.+T*F)
      RETURN
      END
```